

Experimental Study of Cold-Formed Ferritic Stainless Steel Hollow Sections

S. Afshan¹ and L. Gardner²

Abstract: Stainless steel is gaining increasing usage in construction owing to its durability, favorable mechanical properties and its aesthetic appearance, with the austenitic grades being the most commonly utilized. Austenitic stainless steels have a high nickel content (8%-11%), resulting in high initial material cost and significant price fluctuations; this, despite its desirable properties, represents a considerable disadvantage in terms of material selection. Ferritic stainless steels, having no or very low nickel content, may offer a more viable alternative for structural applications, reducing both the level and variability of the initial material cost, while maintaining adequate corrosion resistance. There is currently limited information available on the structural performance of this type of stainless steel. Therefore, to overcome this limitation, a series of material, cross-section and member tests have been performed, covering both the standard EN 1.4003 grade (similar to the chromium weldable structural steel 3Cr12) and the EN 1.4509 grade (441), which has improved weldability and corrosion resistance. In total, twenty tensile coupon tests, sixteen compressive coupon tests, eight stub column tests, sixteen flexural buckling tests and eight in-plane bending tests were carried out. Precise measurements of the geometric properties of the test specimens, including the local and global geometric imperfections were also made. The experimental results are used to assess the applicability of the current European (EN 1993-1-4:2006) and North American (SEI/ASCE-8:2002) provisions to ferritic stainless steel structural components. In addition, the relative structural performance of ferritic stainless steel to

¹ PhD Student, Dept. of Civil and Environmental Engineering, South Kensington Campus, Imperial College London, London SW7 2AZ, U.K. (corresponding author) E-mail: sheida.afshan06@imperial.ac.uk

² Reader, Dept. of Civil and Environmental Engineering, South Kensington Campus, Imperial College London, London SW7 2AZ, U.K. E-mail: leroy.gardner@imperial.ac.uk

that of more commonly used stainless steel grades is also presented, showing ferritic stainless steel to be an attractive choice for structural applications.

CE Database subject headings: Beams; Buckling; Cold-formed steel; Column; Cross-section; Design; Hollow sections; Laboratory tests; Stainless steel.

Introduction

The physical and mechanical characteristics of stainless steel such as high strength, stiffness and ductility, weldability, durability, good fire resistance and ready re-use and recycling make it suitable for a range of architectural and structural applications. The austenitic EN 1.4301 and EN 1.4401 (304 and 316) grades, containing 17-18% chromium and 8-11% nickel, are most commonly used in construction. Both grades have a minimum specified design strength (0.2% proof strength) of 210-240 N/mm² (EN 10088-4 2009). The high nickel content of the austenitic grades provides a number of positive attributes, such as very good ductility and elevated temperature performance, but the resulting high initial material cost is a significant disincentive for material selection.

Ferritic stainless steels, having no or very low nickel content, may offer a more viable alternative for structural applications, due to their lower initial material cost and improved price stability. The main alloying element is chromium, with contents typically between 11 and 18% (EN 10088-4 2009). These steels are easier to work and machine than the austenitic grades and have a higher yield strength in the annealed condition of 250-330 N/mm². Furthermore, by varying the chromium content (10.5%-29%), and with additions of other alloying elements, the required corrosion resistance for a wide range of structural applications and operating environments can be achieved. Stabilized ferritic grades, with additions of titanium and niobium alloying elements, such as EN 1.4509 (441) and EN 1.4521 (444) are broadly similar in terms of corrosion resistance to the EN 1.4301 and EN 1.4401 austenitic grades.

Ferritic stainless steel has been widely used in various applications in the automotive industry, road and rail transport, power generation and mining, though its structural usage has remained relatively scarce. Despite some previous research (van den Berg 2000) and inclusion of the three traditional ferritic grades – EN 1.4003 (similar to chromium weldable structural steel 3Cr12), EN 1.4016 (430) and EN 1.4512 (409) – in Eurocode 3: Part 1.4 (2006), their structural performance requires further verification, particularly for the case of hollow sections. Hence, the focus of the present paper is to describe a comprehensive laboratory testing program on grades EN 1.4003 and EN 1.4509 stainless steel square and rectangular hollow sections (SHS and RHS, respectively), which has been recently conducted at Imperial College London. To determine material properties, a total of twenty tensile coupon tests, including both flat and corner specimens, and sixteen compressive coupon tests have been performed. At cross-section level, eight stub column tests and eight in-plane bending tests, including 3-point bending and 4-point bending configurations, have been carried out. At member level, sixteen column flexural buckling tests have been conducted. The experimental results obtained are reported, analyzed and compared to the results of tests performed on other stainless steel grades. Finally, design recommendations suitable for incorporation into European (EN 1993-1-4 2006) and North American (SEI/ASCE-8 2002) standards have been proposed.

Experimental Studies

Introduction

A laboratory testing program comprising thirty six material tests, eight stub column tests, eight bending tests and sixteen flexural buckling tests has been conducted at Imperial College London to investigate the structural performance of cold-formed ferritic stainless steel tubular structural elements. Four section sizes were examined, namely RHS 120×80×3, RHS 60×40×3, SHS 80×80×3 and SHS 60×60×3. The first three sections were of the standard EN 1.4003 grade, while

the SHS 60×60×3 was grade EN 1.4509, which has improved weldability and corrosion resistance. The chemical compositions and the tensile properties of the coil material from which the specimens were formed, as provided by the mill certificates, are presented in Tables 1 and 2 respectively. No chemical composition details were available for the grade EN 1.4509 SHS 60×60×3 specimens. The notation employed in Table 2 is as follows: $\sigma_{0.2}$ is the 0.2% proof stress, $\sigma_{1.0}$ is the 1% proof stress, σ_u is the ultimate tensile stress and ϵ_f is the tensile strain at fracture.

Material Tests

A series of tensile and compressive coupon tests were conducted to determine the basic engineering stress-strain response of the SHS and RHS ferritic specimens. All material was extracted from the same lengths of tube as the stub column, long column and beam specimens. One tensile flat and one compressive flat coupon were machined from each of the four faces of the SHS and RHS specimens in the longitudinal direction, resulting in a total of sixteen tensile coupon tests and sixteen compressive coupon tests. All tensile coupons were parallel necked specimens with a neck length of 150 mm and width of 20 mm, while the compressive coupons were of nominal dimensions 72 × 16 mm. Stainless steel exhibits pronounced strain hardening, resulting in the corner regions of cold-formed sections having a higher strength than that of the flat material (Ashraf et al. 2005). In order to investigate the extra degree of strength in the cold-worked corner regions, tensile tests on corner coupons, with nominal length of 320 mm, extracted from the curved portions of each of the cold-formed sections, were also conducted.

The tests were performed using an Instron 8802 250 kN hydraulic testing machine, in accordance with EN 10002-1 (2001). Strain control was used to drive the testing machine at a strain rate of 0.002 %/s up to the 0.2% proof stress and 0.005 %/s until fracture for the tensile coupon tests. A uniform displacement rate of 0.07 mm/min was used for the compressive coupon tests. For the tensile coupon tests, an optical extensometer was used to measure the longitudinal strain over a

gauge length of 100 mm while two linear electrical resistance strain gauges attached to the edges of the compressive coupons were used to measure the strain. Static loads were obtained at key stages by holding the cross head of the testing machine for a duration of 2 minutes to allow stress relaxation to take place. Buckling of the compressive coupons was prevented by means of a bracing jig. Load, strain and other relevant variables were all recorded at one second intervals using the fully integrated modular software package, Blue-hill 2.

The obtained material data for each specimen are given in Table 3, while the weighted average (based on face width) tensile and compressive material properties of each section are given in Tables 4 and 5, respectively. The coupon designation begins with the section size, e.g. SHS 80×80×3, followed by the test type – TF for tensile flat, CF for compressive flat and TC for tensile corner – and finally the section face number (1, 2, 3 or 4), as explained in Fig. 1. The material parameters reported in Tables 3 and 4 are the Young's modulus E , the static 0.2% proof stress $\sigma_{0.2}$, the static 1% proof stress $\sigma_{1.0}$, the static ultimate tensile stress σ_u , the plastic strain at fracture ϵ_f , (based on elongation over the standard gauge length equal to $5.65\sqrt{A_c}$, where A_c is the cross-sectional area of the coupon) and the strain hardening exponents n and $n'_{0.2,1.0}$ used in the compound Ramberg-Osgood material model (Mirambell and Real 2000; Rasmussen 2003 and Ashraf et al. 2006). The early region of the stress-strain curve which was affected by the initial curvature of the coupons was not considered for the calculation of the Young's modulus. The measured tensile stress-strain curves, up to 1% tensile strain, are depicted in Figs 2-5.

Stub column tests

Stub column tests on four ferritic stainless steel sections, RHS 120×80×3, RHS 60×40×3, SHS 80×80×3 and SHS 60×60×3, were performed. Two repeated concentric compression tests were carried out for each section size. Stub column lengths were selected to be short enough to avoid overall flexural buckling, but still long enough to provide a representative pattern of geometric imperfections and residual stresses (Galambos 1998). The chosen nominal lengths were equal to three times the larger nominal cross-section dimension for the RHS 120×80×3, SHS 80×80×3 and SHS 60×60×3 specimens. A shorter length, equal to two times the larger nominal cross-section dimension, was employed for the RHS 60×40×3 specimens, since evidence of global buckling was observed in the failure modes of longer specimens.

The ends of the stub column specimens were milled flat and square to ensure uniform loading distribution during testing. The specimens were compressed between parallel platens in an Instron 3500 kN hydraulic testing machine. The test set-up was displacement controlled. The instrumentation consisted of one linear variable displacement transducer (LVDT) to measure the end shortening between the flat platens, a load cell to accurately record the applied load and four linear electrical resistance strain gauges. The strain gauges were affixed to each specimen at mid-height and at a distance four times the material thickness from the corners. All data, including load, displacement, strain and voltage, were recorded at one second intervals using the data acquisition equipment DATASCAN and logged using DSLOG computer package.

The average measured geometric dimensions of each stub column specimen are provided in Table 6, where L is the stub column length, h is the section depth, b is the section width, t is the thickness and r_i is the average internal corner radius (see Fig. 1). Initial local geometric imperfection magnitudes were not measured specifically for each test specimen, but were measured over a representative 800 mm length of each section size, following the procedures of Schafer and Peköz (1998). The maximum deviations from a flat datum were recorded for the four faces of each section, and then averaged to give the imperfection magnitudes w_0 reported in Table 6.

The static ultimate load N_u and the corresponding end shortening at ultimate load δ_u are given in Table 7. All test specimens failed by local buckling of the flat elements comprising the section. Fig. 6 shows typical failure modes. Tests were continued beyond the ultimate load and the post ultimate response was recorded. Full load-end shortening curves for the tested specimens are depicted in Fig. 7. Relevant guidelines provided by the Centre for Advanced Structural Engineering (1990) were used to eliminate elastic deformation of the end platens from the end shortening measurements. Hence the true deformations of the stub columns were determined and used throughout the study.

Beam tests

A total of eight in-plane bending tests, in two configurations, were conducted to investigate the cross-section response of SHS and RHS ferritic stainless steel beams under constant moment (four-point bending) and a moment gradient (three-point bending). All specimens had a total length of 1700 mm and were simply supported between two steel rollers, which were placed 100 mm inwards from the ends of the beams and allowed axial displacement of the beam's ends, resulting in a span of 1500 mm.

The tested beams were loaded symmetrically, in an Instron 2000 kN hydraulic testing machine, at the third points and at mid-span for the four-point bending (4PB) and the three-point bending (3PB) arrangements respectively, as shown in Figs 8 and 9. String potentiometers were located at the loading points to measure the vertical deflections, and, for the three-point bending tests, two inclinometers were also positioned at each end of the beam specimens to measure end rotations. Linear electrical resistance strain gauges were affixed to the extreme tensile and compressive fibers of the section at mid-span and at 100 mm distance from the mid-span for the four-point bending and for the three-point bending tests respectively. Wooden blocks were placed within the tubes at the loading points to prevent web crippling. The test set-up was displacement

controlled at a rate of 2 mm/min. Load, displacement, strain, end rotation and input voltage were all recorded using the data acquisition equipment DATASCAN and logged using DSLOG computer package.

Average measured dimensions of the beam specimens, together with the maximum local imperfections w_0 , are reported in Table 8. The static ultimate test bending moment M_u and the cross-section rotation capacity R are reported in Table 9. The obtained moment-curvature and mid-span moment-rotation curves from the four-point and three-point bending tests are shown in Figs 10 and 11 respectively, where M_u is the ultimate test moment, M_{pl} is the plastic moment capacity, θ is the mid-span rotation – taken as the sum of the two end rotations from the inclinometer measurements –, θ_{pl} is the elastic component of the rotation at M_{pl} , κ is the curvature and κ_{pl} is the elastic curvature corresponding to M_{pl} . The curvature was evaluated using Eq. (1), where $D_{mid-span}$ is the vertical deflection at mid-span, $D_{average}$ is the average vertical displacement at the loading points and $L_{mid-span}$ is the length between the loading points. Rotation capacity was calculated as $R = (\kappa_u/\kappa_{pl}) - 1$ and $R = (\theta_u/\theta_{pl}) - 1$ for the four-point bending and three-point bending tests respectively, where κ_u (θ_u) is the curvature (rotation) at which the moment-curvature (moment-rotation) curve falls below M_{pl} on the descending branch and κ_{pl} (θ_{pl}) is the elastic curvature (rotation) corresponding to M_{pl} on the ascending branch. All test specimens failed by local buckling of the compression flange.

$$\kappa = \frac{8 \left(D_{mid-span} - D_{average} \right)}{4 \left(D_{mid-span} - D_{average} \right)^2 + L_{mid-span}^2} \quad (1)$$

Flexural buckling tests

Column tests on ferritic stainless steel members, with the same nominal cross-section dimensions as examined as stub columns and beams – RHS 120×80×3, RHS 60×40×3, SHS 80×80×3 and

SHS 60×60×3 – were carried out to investigate the flexural buckling response of SHS and RHS pin-ended compression members under axial loading. Four different column lengths of nominal dimensions 1.1 m, 1.6 m, 2.1 m and 2.6 m were tested for each cross-section, providing a spectrum of non-dimensional member slenderness $\bar{\lambda}$, defined in accordance with EN 1993-1-4 (2006) – see Eq. (2) – , ranging from 0.31 to 2.33.

$$\bar{\lambda} = \sqrt{\frac{A\sigma_{0.2}}{N_{cr}}} \quad (2)$$

where A is the cross-sectional area, taken as the gross cross-sectional area for fully effective sections and the effective cross-sectional area A_{eff} for slender sections, $\sigma_{0.2}$ is the 0.2% proof stress and N_{cr} is the elastic buckling load of the column.

Measurements of the geometries of the column specimens and the initial global geometric imperfections were conducted prior to testing and are provided in Table 10, where symbols are as previously defined in Fig. 1 and ω_0 is the measured global imperfection amplitude in the axis of buckling. The general test set-up configuration is depicted in Fig 12. The specimens were loaded in an Instron 2000 kN hydraulic testing machine through hardened steel knife-edges at both ends to provide pinned end conditions about the axis of buckling and fixed conditions about the orthogonal axis, as shown in Fig 12. Displacement control was employed to drive the hydraulic machine at a constant rate of 0.5 mm/min. For column specimens where the measured global imperfection ω_0 was less than $L/1500$, where L is the pin-ended column buckling length taken as the total distance between the steel knife-edges, an eccentricity of loading was applied such that the combined imperfection plus eccentricity was equal to $L/1500$. For other tests, the load was applied concentrically since the measured global imperfections were greater than $L/1500$.

The instrumentation consisted of a string potentiometer to measure the mid-height lateral deflection in the axis of buckling, inclinometers positioned at each end of the members to measure the end rotations about the axis of buckling and four linear electrical resistance strain gauges affixed to the extreme tensile and compressive fibers of the section at mid-height and at a distance of four times the material thickness from the corners. Applied load and vertical displacement were obtained directly from the loading machine. Load, strain, lateral and vertical displacements, end rotations and input voltage were all recorded using the data acquisition equipment DATASCAN and logged using DSLOG computer package. All data were recorded at one second intervals. The failure modes of the columns involved overall flexural buckling and combined local and overall buckling. The full load-lateral displacement curves were recorded and are shown in Figs. 13 and 14 for the SHS and RHS specimens, respectively. Key results from the tests, including the static ultimate load N_u and the lateral displacement at ultimate load ω_u are reported in Table 11.

Analysis of results and design recommendations

Cross-section classification

In the European structural stainless steel design standard Eurocode 3: Part 1-4 (2006) the concept of cross-section classification is employed for the treatment of local buckling. The method assumes elastic-perfectly plastic material behavior for stainless steel as for carbon steel in Eurocode 3: Part 1-1 (2005), with the yield stress taken as the 0.2% proof stress. The classification of plate elements in cross-sections, is based on the width-to-thickness ratio (b/t), the material properties $[(235/f_y)(E/210000)]^{0.5}$, the edge support conditions (i.e. internal or outstand referred to as stiffened and unstiffened respectively in the North American specification) and the form of the applied stress field. The overall cross-section classification is assumed to relate to its most slender constituent element. The definition of the four classes employed in Eurocode 3: Part 1.4

is as follows: Class 1 cross-sections are fully effective under pure compression and capable of reaching and maintaining their full plastic moment M_{pl} in bending; Class 2 cross-sections have a somewhat lower deformation capacity, but are also fully effective in pure compression and capable of reaching their full plastic moment in bending; Class 3 cross-sections are fully effective in pure compression, but local buckling prevents attainment of the full plastic moment in bending, limiting its bending resistance to the elastic moment M_{el} ; Class 4 cross-sections are characterized as slender and cannot reach their nominal yield strength in compression or their elastic moment capacity in bending – to reflect this, regions of the sections rendered ineffective by local buckling are removed and section properties are calculated on the basis of the remaining cross-section.

The North American SEI/ASCE-8 (2002) specification for the design of cold-formed stainless steel structures employs a similar approach for cross-sections in compression and calculates the moment capacity either on the basis of initiation of yielding (procedure I) or on the basis of the inelastic reserve capacity (procedure II). Procedure I assumes a linear stress distribution throughout the cross-section with the yield stress being the maximum allowable stress. A maximum slenderness limit, equivalent to the Eurocode 3: Part 1.4 Class 3 limit, is provided, beyond which loss of effectiveness due to local buckling needs to be accounted for through the use of effective section properties. The additional inelastic reserve capacity associated with stockier cross-sections, up to a maximum slenderness limit equivalent to the Eurocode 3: Part 1.4 Class 1 limit, may be utilized through the application of the procedure II design method, provided certain criteria regarding web slenderness, cross-section geometry, shear stresses and the elimination of other possible failure modes are satisfied.

In this section, the experimental results are used to assess the applicability of the cross-section classification limits provided in the current European (EN 1993-1-4 2006) and North American (SEI/ASCE-8 2002) standards to ferritic stainless steel internal elements. In addition, the proposed limits of Gardner and Theofanous (2008), which are derived and statistically validated

based on all relevant published test data on stainless steel, are also considered. The measured weighted average material properties from the flat tensile coupon tests for each cross-section were utilized throughout the analyses.

Both the stub column tests results and the bending tests results have been utilized to assess the suitability of the Class 3 slenderness limit for internal elements in compression. Figs 15 and 16 show the relevant response characteristics ($N_u / A\sigma_{0.2}$ and M_u / M_{el}), where N_u and M_u are the ultimate test load and moment respectively and M_{el} is the conventional elastic moment capacity, given as the product of the elastic section modulus and the yield strength, plotted against the slenderness parameter $c/t\epsilon$ of the most slender constituent element in the cross-section, where c is the compressed flat width, t is the element thickness and $\epsilon = [(235/f_y)(E/210000)]^{0.5}$ as defined in EN 1993-1-4 (2006). In determining the most slender element, due account of the stress distribution and element support conditions have been made through the buckling factor k_σ , as defined in EN 1993-1-5 (2006). The Class 3 limit specified in Eurocode 3: Part 1-4 is 30.7, whereas the equivalent Class 3 limit of the SEI/ASCE-8 is 38.2. The Class 3 slenderness limit proposed by Gardner and Theofanous (2008) is 37, which is very close to the slenderness limit of 38.3 codified in SEI/ASCE-8 (2002). From Figs 18 and 19, it may be concluded that the current Class 3 limit given in EN 1993-1-4 (2006) is applicable to ferritic stainless steel internal elements under compression but is rather conservative, while the SEI/ASCE-8 (2002) limit and the proposed limit of Gardner and Theofanous (2008) allow more efficient exploitation of the material.

The Class 2 slenderness limits specified in EN 1993-1-4 (2006) and proposed by Gardner and Theofanous (2008), together with the bending test results are shown in Fig. 17, where the test ultimate moment capacity M_u has been normalized by the plastic moment capacity M_{pl} , given as the product of the plastic section modulus and the yield strength, and plotted against the slenderness parameter $c/t\epsilon$ of the most slender constituent element in the cross-section. In Fig.

18, the rotation capacity R is plotted against the slenderness parameter c/t_e of the most slender constituent element in the cross-section. In the absence of a codified deformation capacity requirement for Class 1 stainless steel cross-sections, the equivalent carbon steel rotation capacity requirement of $R = 3$ (Sedlacek and Feldmann 1995) has been used herein. From Fig. 22, the EN 1993-1-4 (2006) Class 2 limit of 26.7 may be seen to be safe, whereas the proposed limit of 35 (Gardner and Theofanous 2008) provides more economical structural design. The SEI/ASCE-8 (2002) equivalent Class 1 limit, which is the same as the corresponding limit proposed by Gardner and Theofanous (2008), appears optimistic for ferritic stainless steel and the EN 1993-1-4 (2006) provisions may be adopted.

Flexural buckling

The Eurocode 3: Part 1-4 (2006) design approach for flexural buckling of compression members is based on the Perry-Robertson buckling formulation with a linear imperfection parameter $\eta = \alpha(\bar{\lambda} - \bar{\lambda}_0)$, where α and $\bar{\lambda}_0$ are constants accounting for the geometric imperfections and residual stresses effects on the column strength. The design buckling curves were derived by calibration against the then available stainless steel test data to provide a suitably conservative fit for design purposes. A single buckling curve is provided for cold-formed open and rolled tubular sections of austenitic, duplex and ferritic stainless steel grades. For simplicity, to avoid the need for iteration, and for consistency with the carbon steel approach, no explicit allowance is made for the effect of gradual material yielding in the member buckling formulations. In contrast, the SEI/ASCE-8 (2002) provisions for stainless steel column design allow for the non-linear stress-strain response through the use of the tangent modulus E_t , corresponding to the buckling stress, in place of the initial modulus E in the buckling formulations, which involves an iterative design approach.

In addition to the iterative method from the SEI/ASCE-8 (2002) specification, an alternative explicit design procedure is also provided in AS/NZS 4673 (2001) Standard for Cold-Formed Stainless Steel Structures. The method is essentially the same as the Eurocode 3: Part 1-4 (2006) formulation for flexural buckling of compression members, except that a non-linear expression is used for the imperfection parameter instead of the linear expression adopted in Eurocode 3: Part 1-4 (2006). In addition, a total of six buckling curves are provided for different stainless steel grades, austenitic (EN 1.4301, 1.4401, 1.4306 and 1.4404), ferritic (EN 1.4512, 1.4003 and 1.4016) and duplex (EN 1.4462). In this section, the results of the ferritic stainless steel column flexural buckling tests performed herein are examined and compared with the current column design provisions adopted in the European, North American and Australian/New Zealand standards.

In Fig. 19, the test ultimate loads normalized by the corresponding tensile and compressive squash loads, based on the gross cross-sectional area for fully effective sections and the effective cross-sectional area A_{eff} for slender sections, have been plotted against the non-dimensional slenderness $\bar{\lambda}$ as defined in Eq (2). Stub column test data are also included. The SEI/ASCE-8 buckling curves, based on the mean measured tensile and compressive flat weighted average material properties of the tested sections, together with the EC3: Part 1-4 buckling curve for cold-formed hollow sections, with the imperfection factor $\alpha = 0.49$ and $\bar{\lambda}_0 = 0.4$ as specified in Eurocode 3: Part 1-4 (2006), are also depicted. The AS/NZS buckling curve for grade EN 1.4003 is also included. To allow suitable comparison with the test data, measured geometry and material properties are adopted and all codified factors of safety are set to unity.

As shown in Fig. 19, the SEI/ASCE-8 curves are the highest over the majority of the slenderness range and generally over predict the test results. The AS/NZS curve is below the EC4: Part 1-4 buckling curve in the low and intermediate slenderness ranges, with both curves meeting at a

slenderness value of about 1.2 and converging towards the elastic buckling curve at higher slenderness. Overall, the EC3: Part 1.4 buckling curve provides a better representation of the member buckling resistance over the full slenderness range with the exception of the data point with $\bar{\lambda} = 0.53$ (tensile) which is better predicted by the AS/NZS curve. Overall, it may be concluded that the current European and AS/NZS codified provisions for the design of stainless steel columns are applicable to ferritic stainless steel columns.

Comparison with other stainless steel grades

Test data collected from the literature (Rasmussen and Hancock 1993a, Rasmussen and Hancock 1993b, Talja and Salmi 1995, Ala-Outinen and Oksanen 1997, Kuwamura 2003, Liu and Young 2003, Young and Liu 2003, Gardner and Nethercot 2004a, Gardner and Nethercot 2004b, Real and Mirambell 2005, Young and Lui 2005, Zhou and Young 2005, Gardner et al. 2006, Young and Lui 2006, Theofanous and Gardner 2009, Gardner and Theofanous 2010, Theofanous and Gardner 2010) on austenitic, duplex and lean duplex stainless steel SHS and RHS specimens have been utilized to compare with the test results generated herein and to assess the relative performance of various stainless steel grades. In Fig. 20, the reported ultimate load capacity from stub column tests have been normalized by the respective cross-sectional area and plotted against the c/t ratio of the most slender element in the section. The bending tests results reported herein were also compared to tests on other stainless steel grades as shown in Fig. 21, where the ultimate moment capacity normalized by the respective plastic section modulus is plotted against the c/t ratio of the compression flange of the cross-section. The collected column flexural buckling data are presented in Fig. 22, where the member slenderness is calculated based on the geometric properties of the gross cross-sections. The experimental data presented in Figs 25-27 exhibit the general anticipated trend of reducing failure stress with increasing slenderness. The vertical scatter for a given slenderness reflects the variation in material strength between the tested specimens. Overall, of the grades considered, lean duplex specimens generally show the highest

failure stress, which is in line with the high yield strength associated with this material, while the results of the other grades overlap.

Conclusions

A laboratory testing program has been conducted at Imperial College London to investigate the structural performance of cold-formed ferritic stainless steel tubular structural elements. Eight stub column tests, sixteen flexural buckling tests, eight beam tests and a total of thirty six material tests have been reported herein. The experimental results were used to assess the applicability of the European (EN 1993-1-4 2006) and North American (SEI/ASCE-8 2002) provisions to ferritic stainless steel structural components. It was concluded that the current Class 3 slenderness limits provided in EN 1993-1-4 (2006) is applicable to ferritic stainless steel internal elements under compression, while the SEI/ASCE-8 (2002) equivalent limit and the proposed limit of Gardner and Theofanous (2008) allow greater design efficiency. Similarly, the EN 1993-1-4 (2006) Class 2 limit was considered to be safe whereas the more relaxed limit of Gardner and Theofanous (2008) provides more economical structural design. The SEI/ASCE-8 (2002) equivalent Class 1 limit and that proposed by Gardner and Theofanous (2008) appeared to be optimistic for ferritic stainless steel; hence, the EN 1993-1-4 (2006) limit was recommended in this paper. The EC3: Part 1.4 and AS/NZS column buckling curves were shown to provide a good overall representation of the buckling resistance exhibited by the test specimens; hence, it was recommended that these provisions are applicable to ferritic stainless steel columns. The laboratory test results on ferritic stainless steel were also compared to test results on austenitic, duplex and lean duplex stainless steel SHS and RHS specimens collected from the literature. Overall, ferritic stainless steel shows similar structural performance to other commonly used stainless steel grades and at a lower material cost, making it an attractive choice for structural applications.

Acknowledgements

The authors are grateful to the Outokumpu Research Foundation and the Steel Construction Institute for their financial contributions to the project and Stalatube Finland for providing the test specimens, and would like to thank Gordon Herbert and Angeliki Ntikmpasani for their assistance during the experimental investigations.

Notation

| | |
|------------------|--------------------------------|
| A | Cross-sectional area |
| A_{eff} | Effective cross-sectional area |
| A_c | Coupon cross-sectional area |
| b | Width |
| E | Young's modulus |
| h | Depth |
| I | Second moment of area |
| i | Radius of gyration |
| k_{σ} | Buckling coefficient |
| L | Member length |
| L_{cr} | Column buckling length |
| M_{el} | Elastic moment capacity |
| M_{pl} | Plastic moment capacity |
| M_u | Test ultimate moment |
| N | Load |
| N_b | Column buckling load |
| N_u | Test ultimate load |
| N_{cr} | Elastic buckling load |

| | |
|-----------------|---|
| N_y | Yield load |
| n | Strain hardening component used in Ramberg-Osgood model |
| $n'_{0.2,1.0}$ | Strain hardening component used in compound Ramberg-Osgood model |
| RHS | Rectangular hollow section |
| R | Rotation capacity |
| r_i | Internal corner radius |
| SHS | Square hollow section |
| t | Thickness |
| w_0 | Maximum measured local imperfection |
| δ_u | Stub column end shortening at ultimate load |
| ε | Material factor defined in EN 1993-1-4 (2006) |
| ε_f | Strain at fracture |
| θ | Rotation |
| θ_u | Total rotation at mid-span when the moment-rotation curve falls below M_{pl} on the descending branch |
| θ_{pl} | Elastic part of the total rotation at mid-span when M_{pl} is reached on the ascending branch |
| κ | Curvature |
| κ_u | Total curvature at mid-span when the moment-curvature curve falls below M_{pl} on the descending branch |
| κ_{pl} | Elastic part of the total curvature at mid-span when M_{pl} is reached on the ascending branch |
| $\bar{\lambda}$ | Member slenderness |
| σ | Stress |
| $\sigma_{0.2}$ | 0.2 % proof stress |

| | |
|----------------|---------------------------------------|
| $\sigma_{1.0}$ | 1.0 % proof stress |
| σ_u | Ultimate tensile stress |
| ω | Lateral deflection |
| ω_0 | Initial global imperfection amplitude |
| ω_u | Lateral deflection at ultimate load |

References

Ala-Outinen, T. and Oksanen, T. (1997). “Stainless steel compression members exposed to fire.” Research Note 1864. Finland: VTT Building Technology.

American Society of Civil Engineers (ASCE). (2002). *Specification for the design of cold-formed stainless steel structural members*, SEI/ASCE 8-02, Reston.

Ashraf, M., Gardner, L. and Nethercot, D. A. (2005). “Strength enhancement of the corner regions of stainless steel cross-sections”. *J. Constr. Steel Res.*, 61(1), 37-52.

Ashraf, M., Gardner, L. and Nethercot, D. A. (2006). “Finite element modelling of structural stainless steel cross-sections.”. *Thin-Walled Struct.*, 44(10), 1048-1062.

Centre for Advanced Structural Engineering. (1990). “Compression tests of stainless steel tubular columns.”. Investigation Report S770. University of Sydney.

European Committee for standardization (CEN). (2005). *Eurocode 3: Design of steel structures - Part 1-1: General rules and rules for buildings*, EN 1993-1-1, Brussels, Belgium.

European Committee for standardization (CEN). (2006). *Eurocode 3: Design of steel structures - Part 1-4: General rules- Supplementary rules for stainless steel*, EN 1993-1-4, Brussels, Belgium.

European Committee for standardization (CEN). (2006). *Eurocode 3: Design of steel structures - Part 1-5: Plated structural elements, EN 1993-1-5*, Brussels, Belgium.

European Committee for standardization (CEN). (2001). *Metallic materials - Tensile testing - Part 1: Method of test at ambient temperature, EN 10002-1*, Brussels, Belgium.

European Committee for standardization (CEN). (2009). *Stainless steels - Part 4: Technical delivery conditions for sheet/plate and strip of corrosion resisting steels for general purposes. EN 10088-4*. Brussels, Belgium.

Galambos, TV. (1998). “*Guide to Stability Design Criteria for Metal Structures.*”, 5th Ed., J. Wiley & Sons, New York.

Gardner, L. and Nethercot, D. A. (2004a). “Experiments on stainless steel hollow sections-Part 1: Material and cross-sectional behavior.” *J. Constr. Steel Res.*, 60(9), 1291-1318.

Gardner, L. and Nethercot, D. A. (2004b). “Experiments on stainless steel hollow sections, Part 2: Member behaviour of columns and beams.” *J. Constr. Steel Res.*, 60(9), 1319–1332.

Gardner, L., Talja, A. and Baddoo, N. R. (2006), “Structural design of high-strength austenitic stainless steel.” *Thin-Walled Struct.*, 44(5), 517-528.

Gardner, L. and Theofanous, M. (2008). “Discrete and continuous treatment of local buckling in stainless steel elements.” *J. Constr. Steel Res.*, 64(11), 1207-1216.

Gardner, L. and Theofanous, M. (2010). “Plastic Design of Stainless Steel Structures.” *Proc., Int. Colloquia on Stability and Ductility of Steel Structures*, Rio de Janeiro, Brazil, 665-672.

Kuwamura, H. (2003). “Local buckling of thin-walled stainless steel members.” *Steel Structures.*, 3(3), 191–201.

Liu, Y. and Young, B. (2003). “Buckling of stainless steel square hollow section compression members.” *J. Constr. Steel Res.*, 59(2), 165-177.

Mirambell, E. and Real, E. (2000). “On the calculation of deflections in structural stainless steel beams: an experimental and numerical investigation.” *J. Constr. Steel Res.*, 54(1), 109-133.

Rasmussen, K. J. R. and Hancock, G. J. (1993a). “Design of cold-formed stainless steel tubular members. I: Columns” *J. Struct. Eng., ASCE*, 119(8), 2349–2367.

Rasmussen, K. J. R. and Hancock, G. J. (1993b). “Design of cold-formed stainless steel tubular members II: Beams.” *J. Struct. Eng., ASCE*, 119(8), 2368–2386.

Rasmussen, K. J. R. and Rondal, J. (2000). “Column curves for stainless steel alloys.” *J. Constr. Steel Res.*, 54(1), 89-107.

Rasmussen, K. J. R. (2003). “Full-range stress–strain curves for stainless steel alloys.” *J. Constr. Steel Res.*, 59(1), 47-61.

Real, E. and Mirambell, E. (2005). “Flexural behavior of stainless steel beams.” *Eng. Struct.*, 27(10), 1465–1475.

Schafer, B. W. and Peköz, T. (1998). “Computational modeling of cold-formed steel: characterizing geometric imperfections and residual stresses.” *J. Constr. Steel Res.*, 47(3), 193-210.

Sedlacek, G. and Feldmann, M. (1995). “The b/t-ratios controlling the applicability of analysis models in Eurocode 3, Part 1.1. Background Document 5.09 for chapter 5 of Eurocode 3, Part 1.1.”, Aachen.

Talja, A. and Salmi, P. (1995). "Design of stainless steel RHS beams, columns and beam-columns." Research note 1619. Finland: VTT building technology.

Theofanous, M. and Gardner, L. (2009). "Testing and numerical modeling of lean duplex stainless steel hollow section columns." *Eng. Struct.*, 31(12), 3047-3058.

Theofanous, M. and Gardner, L. (2010). "Experimental and numerical studies of lean duplex stainless steel beams." *J. Constr. Steel Res.*, 66(6), 816-825.

van den Berg, G . J. (2000). "The effect of non-linear stress-strain behavior of stainless steels on member capacity." *J. Struct. Eng.*, 135(1), 135-160.

Young, B. and Liu, Y. (2003). "Experimental investigation of cold-formed stainless steel columns." *J. Struct. Eng., ASCE*, 129(2), 169-176.

Young, B. and Lui, W. M. (2005). "Behavior of cold-formed high strength stainless steel sections." *J. Struct. Eng., ASCE*, 131(11), 1738-1745.

Young, B. and Lui, W. M. (2006). "Tests on cold formed high strength stainless steel compression members." *Thin-Walled Struct.*, 44(2), 224-234.

Zhou, F. and Young, B. (2005). "Tests of cold-formed stainless steel tubular flexural members." *Thin-Walled Struct.*, 43(9), 1325–1337.

Table 1. Chemical composition of grade EN 1.4003 stainless steel specimens

| Section | C (%) | Si (%) | Mn (%) | P (%) | S (%) | Cr (%) | Ni (%) | N (%) |
|--------------|-------|--------|--------|-------|-------|--------|--------|-------|
| RHS 120×80×3 | 0.005 | 0.50 | 1.44 | 0.029 | 0.002 | 11.3 | 0.4 | 0.01 |
| RHS 60×40×3 | 0.010 | 0.37 | 1.46 | 0.029 | 0.003 | 11.2 | 0.5 | 0.01 |
| SHS 80×80×3 | 0.010 | 0.25 | 1.43 | 0.028 | 0.003 | 11.3 | 0.4 | 0.01 |

Table 2. Mechanical properties as stated in the mill certificates

| Section | Grade | $\sigma_{0.2, \text{mill}}$ (N/mm ²) | $\sigma_{1.0, \text{mill}}$ (N/mm ²) | $\sigma_{u, \text{mill}}$ (N/mm ²) | ϵ_f (%) |
|--------------|-----------|--|--|--|------------------|
| RHS 120×80×3 | EN 1.4003 | 346 | 368 | 498 | 42 |
| RHS 60×40×3 | EN 1.4003 | 339 | 360 | 478 | 38 |
| SHS 80×80×3 | EN 1.4003 | 321 | 343 | 462 | 45 |

Table 3. Coupon test results for each specimen

| Specimen reference | E | $\sigma_{0.2}$ | $\sigma_{1.0}$ | σ_u | ϵ_f | <u>R-O coefficients</u> |
|--------------------|---|----------------|----------------|------------|--------------|-------------------------|
|--------------------|---|----------------|----------------|------------|--------------|-------------------------|

| | (N/mm ²) | (N/mm ²) | (N/mm ²) | (N/mm ²) | (%) | n | n' ^{0.2,1.0} |
|------------------|----------------------|----------------------|----------------------|----------------------|-----|------|-----------------------|
| RHS 120×80×3-TF1 | 210000 | 450 | 472 | 477 | 33 | 8.8 | 6.3 |
| RHS 120×80×3-TF2 | 215000 | 385 | 405 | 443 | 40 | 8.0 | 2.3 |
| RHS 120×80×3-TF3 | 218000 | 390 | 413 | 458 | 40 | 11.2 | 2.6 |
| RHS 120×80×3-TF4 | 220000 | 510 | - ^a | 535 | 23 | 12.6 | 8.2 |
| RHS 120×80×3-TC | 226000 | 535 | - ^a | 554 | 13 | 6.0 | - |
| RHS 120×80×3-CF1 | 213000 | 439 | 478 | - | - | 5.6 | 2.4 |
| RHS 120×80×3-CF2 | 215000 | 372 | 415 | - | - | 6.9 | 4.1 |
| RHS 120×80×3-CF3 | 210000 | 362 | 415 | - | - | 5.2 | 3.2 |
| RHS 120×80×3-CF4 | 205000 | 487 | 537 | - | - | 5.3 | 2.5 |
| RHS 60×40×3-TF1 | 220000 | 438 | - ^a | 460 | 18 | 8.0 | 8.2 |
| RHS 60×40×3-TF2 | 225000 | 455 | - ^a | 481 | 28 | 9.4 | 9.8 |
| RHS 60×40×3-TF3 | 210000 | 435 | - ^a | 440 | 32 | 7.3 | 9.9 |
| RHS 60×40×3-TF4 | 225000 | 500 | - ^a | 542 | 21 | 6.4 | 8.9 |
| RHS 60×40×3-TC | 200000 | 545 | - ^a | 597 | 10 | 4.7 | - |
| RHS 60×40×3-CF1 | 215000 | 423 | 465 | - | - | 5.5 | 2.2 |
| RHS 60×40×3-CF2 | 220000 | 425 | 495 | - | - | 7.2 | 2.7 |
| RHS 60×40×3-CF3 | 220000 | 400 | 454 | - | - | 7.6 | 4.3 |
| RHS 60×40×3-CF4 | 210000 | 429 | 486 | - | - | 5.0 | 3.8 |
| SHS 80×80×3-TF1 | 220000 | 435 | - ^a | 440 | 36 | 9.1 | 9.6 |
| SHS 80×80×3-TF2 | 200000 | 425 | 435 | 447 | 36 | 10.1 | 6.2 |
| SHS 80×80×3-TF3 | 210000 | 400 | 418 | 432 | 38 | 7.7 | 3.1 |
| SHS 80×80×3-TF4 | 210000 | 465 | - ^a | 470 | 31 | 7.7 | 10.0 |
| SHS 80×80×3-TC | 220000 | 512 | - ^a | 520 | 11 | 7.8 | - |
| SHS 80×80×3-CF1 | 215000 | 413 | 475 | - | - | 7.4 | 2.4 |
| SHS 80×80×3-CF2 | 210000 | 398 | 443 | - | - | 5.1 | 2.5 |
| SHS 80×80×3-CF3 | 215000 | 375 | 423 | - | - | 7.4 | 2.7 |
| SHS 80×80×3-CF4 | 205000 | 429 | 483 | - | - | 5.4 | 2.7 |
| SHS 60×60×3-TF1 | 220000 | 540 | - ^a | 560 | 14 | 7.2 | 10.4 |
| SHS 60×60×3-TF2 | 220000 | 515 | - ^a | 524 | 20 | 8.6 | 9.9 |
| SHS 60×60×3-TF3 | 223000 | 502 | - ^a | 513 | 19 | 8.0 | 10.3 |
| SHS 60×60×3-TF4 | 210000 | 520 | - ^a | 538 | 13 | 7.4 | 12.5 |
| SHS 60×60×3-TC | 225000 | 580 | - ^a | 665 | 13 | 4.3 | 9.5 |
| SHS 60×60×3-CF1 | 215000 | 492 | 542 | - | - | 6.4 | 4.6 |
| SHS 60×60×3-CF2 | 215500 | 465 | 509 | - | - | 6.5 | 2.3 |
| SHS 60×60×3-CF3 | 210000 | 478 | 524 | - | - | 6.9 | 2.8 |
| SHS 60×60×3-CF4 | 220000 | 497 | 550 | - | - | 5.5 | 2.5 |

Note: ^a ultimate tensile stress preceded the 1% proof stress

Table 4. Weighted average tensile flat material properties

| Specimen reference | ϵ_f | R-O coefficients |
|--------------------|--------------|------------------|
|--------------------|--------------|------------------|

| | E (N/mm ²) | $\sigma_{0.2}$ (N/mm ²) | σ_u (N/mm ²) | (%) | n | n' _{0.2,1.0} |
|--------------|---------------------------|--|------------------------------------|-----|------|-----------------------|
| RHS 120×80×3 | 216000 | 423 | 472 | 34 | 10.2 | 4.9 |
| RHS 60×40×3 | 219300 | 454 | 475 | 24 | 7.8 | 9.2 |
| SHS 80×80×3 | 210000 | 431 | 447 | 35 | 8.7 | 7.2 |
| SHS 60×60×3 | 218300 | 519 | 534 | 16 | 7.8 | 10.8 |

Table 5. Weighted average compressive flat material properties

| Specimen reference | E (N/mm ²) | $\sigma_{0.2}$ (N/mm ²) | $\sigma_{1.0}$ (N/mm ²) | R-O coefficients | |
|--------------------|---------------------------|--|--|------------------|-----------------------|
| | | | | n | n' _{0.2,1.0} |
| RHS 120×80×3 | 211150 | 404 | 4501 | 5.8 | 3.1 |
| RHS 60×40×3 | 217200 | 417 | 475 | 6.4 | 3.3 |
| SHS 80×80×3 | 211250 | 404 | 456 | 6.3 | 2.6 |
| SHS 60×60×3 | 215130 | 483 | 531 | 6.3 | 3.1 |

Table 6. Measured dimensions of the stub column specimens

| Specimen | L (mm) | h (mm) | b (mm) | t (mm) | r _i (mm) | w ₀ (mm) | A (mm ²) |
|------------------|-----------|-----------|-----------|-----------|------------------------|------------------------|-------------------------|
| RHS 120×80×3-SC1 | 362.0 | 119.9 | 80.0 | 2.84 | 3.70 | 0.061 | 1077.9 |
| RHS 120×80×3-SC2 | 362.2 | 120.0 | 80.0 | 2.83 | 3.90 | 0.061 | 1074.3 |
| RHS 60×40×3-SC1 | 122.1 | 59.9 | 40.0 | 2.81 | 3.19 | 0.081 | 508.1 |
| RHS 60×40×3-SC2 | 122.1 | 59.9 | 40.0 | 2.81 | 3.19 | 0.081 | 508.0 |
| SHS 80×80×3-SC1 | 242.0 | 80.1 | 80.1 | 2.83 | 3.67 | 0.087 | 850.8 |
| SHS 80×80×3-SC2 | 242.0 | 80.1 | 80.1 | 2.82 | 3.43 | 0.087 | 849.1 |
| SHS 60×60×3-SC1 | 182.2 | 60.5 | 60.5 | 2.98 | 2.90 | 0.061 | 662.1 |
| SHS 60×60×3-SC2 | 182.2 | 60.5 | 60.6 | 2.90 | 3.10 | 0.061 | 654.8 |

Table 7. Summary of test results for stub columns

| Specimen | Ultimate load N_u (kN) | End Shortening at ultimate load δ_u (mm) |
|------------------|-----------------------------|--|
| RHS 120×80×3-SC1 | 449 | 1.16 |
| RHS 120×80×3-SC2 | 441 | 1.19 |
| RHS 60×40×3-SC1 | 278 | 2.18 |
| RHS 60×40×3-SC2 | 271 | 2.12 |
| SHS 80×80×3-SC1 | 392 | 1.42 |
| SHS 80×80×3-SC2 | 389 | 1.49 |
| SHS 60×60×3-SC1 | 376 | 1.92 |
| SHS 60×60×3-SC2 | 370 | 1.94 |

Table 8. Measured dimensions of the beam specimens

| Specimen | Axis of bending | L (mm) | h (mm) | b (mm) | t (mm) | r_i (mm) | w_0 (mm) |
|------------------|-----------------|--------|--------|--------|--------|------------|------------|
| RHS 120×80×3-4PB | Major | 1500 | 120.0 | 79.9 | 2.84 | 3.78 | 0.061 |
| RHS 60×40×3-4PB | Major | 1500 | 60.2 | 39.9 | 2.86 | 3.15 | 0.081 |
| SHS 80×80×3-4PB | - | 1500 | 80.4 | 80.0 | 2.80 | 3.95 | 0.087 |
| SHS 60×60×3-4PB | - | 1500 | 60.7 | 60.7 | 2.89 | 2.86 | 0.061 |
| RHS 120×80×3-3PB | Major | 1500 | 119.9 | 79.9 | 2.83 | 3.80 | 0.061 |
| RHS 60×40×3-3PB | Major | 1500 | 60.4 | 40.8 | 2.82 | 3.18 | 0.081 |
| SHS 80×80×3-3PB | - | 1500 | 80.5 | 80.2 | 2.81 | 3.81 | 0.087 |
| SHS 60×60×3-3PB | - | 1500 | 60.6 | 60.5 | 2.87 | 2.88 | 0.061 |

Table 9. Summary of test results for beams

| Specimen | Axis of bending | Ultimate moment M_u (kNm) | Rotation capacity R |
|------------------|-----------------|--------------------------------|------------------------|
| RHS 120×80×3-4PB | Major | 20.0 | 1.45 |
| RHS 60×40×3-4PB | Major | 5.3 | > 4.90 |
| SHS 80×80×3-4PB | - | 11.3 | 1.86 |
| SHS 60×60×3-4PB | - | 7.9 | 2.85 |
| RHS 120×80×3-3PB | Major | 21.1 | 1.30 |
| RHS 60×40×3-3PB | Major | 5.9 | > 4.10 |
| SHS 80×80×3-3PB | - | 11.4 | 1.12 |
| SHS 60×60×3-3PB | - | 8.4 | 2.15 |

Table 10. Measured dimensions of the flexural buckling specimens

| Specimen | L (mm) | h (mm) | b (mm) | t (mm) | r _i (mm) | ω ₀ (mm) | A (mm ²) |
|-------------------|-----------|-----------|-----------|-----------|------------------------|------------------------|-------------------------|
| RHS 120×80×3-1077 | 1077 | 120.0 | 79.9 | 2.87 | 3.88 | 0.95 | 1088.0 |
| RHS 120×80×3-1577 | 1577 | 120.0 | 79.9 | 2.81 | 3.57 | 0.96 | 1065.5 |
| RHS 120×80×3-2077 | 2077 | 120.0 | 79.8 | 2.78 | 4.10 | 1.05 | 1053.4 |
| RHS 120×80×3-2577 | 2577 | 119.7 | 79.8 | 2.73 | 3.90 | 1.10 | 1034.3 |
| RHS 60×40×3-1177 | 1177 | 59.9 | 39.9 | 2.79 | 3.21 | 1.12 | 504.3 |
| RHS 60×40×3-1577 | 1577 | 59.9 | 39.8 | 2.72 | 3.40 | 1.09 | 491.3 |
| RHS 60×40×3-2077 | 2077 | 59.9 | 39.9 | 2.79 | 3.21 | 1.05 | 503.5 |
| RHS 60×40×3-2577 | 2577 | 59.9 | 39.9 | 2.76 | 3.36 | 0.95 | 498.8 |
| SHS 80×80×3-1177 | 1177 | 80.1 | 79.9 | 2.78 | 3.85 | 1.35 | 833.2 |
| SHS 80×80×3-1577 | 1577 | 80.1 | 80.0 | 2.79 | 3.59 | 1.15 | 838.2 |
| SHS 80×80×3-2077 | 2077 | 80.0 | 79.8 | 2.79 | 3.97 | 1.05 | 833.4 |
| SHS 80×80×3-2577 | 2577 | 80.1 | 79.8 | 2.78 | 3.48 | 1.05 | 833.2 |
| SHS 60×60×3-1177 | 1177 | 60.4 | 60.4 | 2.85 | 2.90 | 1.25 | 634.9 |
| SHS 60×60×3-1577 | 1577 | 60.6 | 60.5 | 2.82 | 2.93 | 1.15 | 629.6 |
| SHS 60×60×3-2077 | 2077 | 60.5 | 60.4 | 2.86 | 3.02 | 1.10 | 637.3 |
| SHS 60×60×3-2577 | 2577 | 60.6 | 60.6 | 2.91 | 3.09 | 1.15 | 647.8 |

Table 11. Summary of results from column flexural buckling tests

| Specimen | Axis of buckling | N _u (kN) | ω _u (mm) |
|-------------------|------------------|------------------------|------------------------|
| RHS 120×80×3-1077 | Major | 463 | 0.77 |
| RHS 120×80×3-1577 | Major | 382 | 9.36 |
| RHS 120×80×3-2077 | Major | 391 | 7.87 |
| RHS 120×80×3-2577 | Major | 308 | 18.27 |
| RHS 60×40×3-1177 | Minor | 103 | 12.72 |
| RHS 60×40×3-1577 | Minor | 72 | 19.62 |
| RHS 60×40×3-2077 | Minor | 51 | 8.78 |
| RHS 60×40×3-2577 | Minor | 30 | 30.50 |
| SHS 80×80×3-1177 | - | 252 | 9.77 |
| SHS 80×80×3-1577 | - | 273 | 7.75 |
| SHS 80×80×3-2077 | - | 222 | 10.39 |
| SHS 80×80×3-2577 | - | 164 | 18.03 |
| SHS 60×60×3-1177 | - | 214 | 10.82 |
| SHS 60×60×3-1577 | - | 166 | 15.64 |
| SHS 60×60×3-2077 | - | 116 | 23.95 |
| SHS 60×60×3-2577 | - | 82 | 24.82 |

Table of Figures

| | |
|--|----|
| Fig. 1. Location of flat and corner coupons and definition of cross-section symbols | 29 |
| Fig. 2. RHS 120×80×3 tensile stress-strain curves | 29 |
| Fig. 3. RHS 60×40×3 tensile stress-strain curves | 30 |
| Fig. 4. SHS 80×80×3 tensile stress-strain curves | 30 |
| Fig. 5. SHS 60×60×3 tensile stress-strain curves | 31 |
| Fig. 6. Typical stub column failure modes | 31 |
| Fig. 7. Load end-shortening curves for stub columns | 32 |
| Fig. 8. Bending test set-up (4PB) | 32 |
| Fig. 9. Bending test set-up (3PB) | 32 |
| Fig. 10. Normalized moment-curvature results (four-point bending) | 33 |
| Fig. 11. Normalized moment-rotation results (three-point bending) | 33 |
| Fig. 12. Flexural buckling test set up | 34 |
| Fig. 13. SHS 80×80×3 and SHS 60×60×3 load-lateral displacement curves | 35 |
| Fig. 14. RHS 120×80×3 and RHS 60×40×3 load-lateral displacement curves | 35 |
| Fig. 15. Assessment of Class 3 slenderness limits for internal elements in compression (stub column tests) | 36 |
| Fig. 16. Assessment of Class 3 slenderness limits for internal elements in compression (bending tests) | 36 |
| Fig. 17. Assessment of Class 2 slenderness limits for internal compression elements | 37 |
| Fig. 18. Assessment of Class 1 slenderness limits for internal compression elements | 37 |
| Fig. 19. Flexural buckling test results and code comparisons | 38 |
| Fig. 20. Performance of stub columns of various stainless steel grades | 38 |
| Fig. 21. Performance of beams of various stainless steel grades | 39 |
| Fig. 22. Performance of columns of various stainless steel grades | 39 |

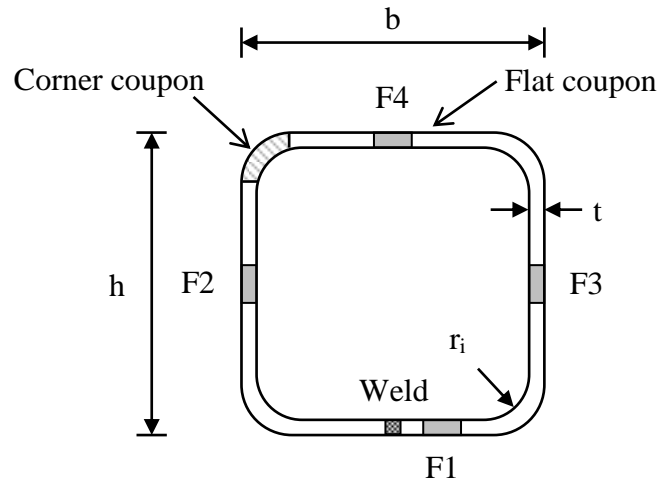


Fig. 1. Location of flat and corner coupons and definition of cross-section symbols

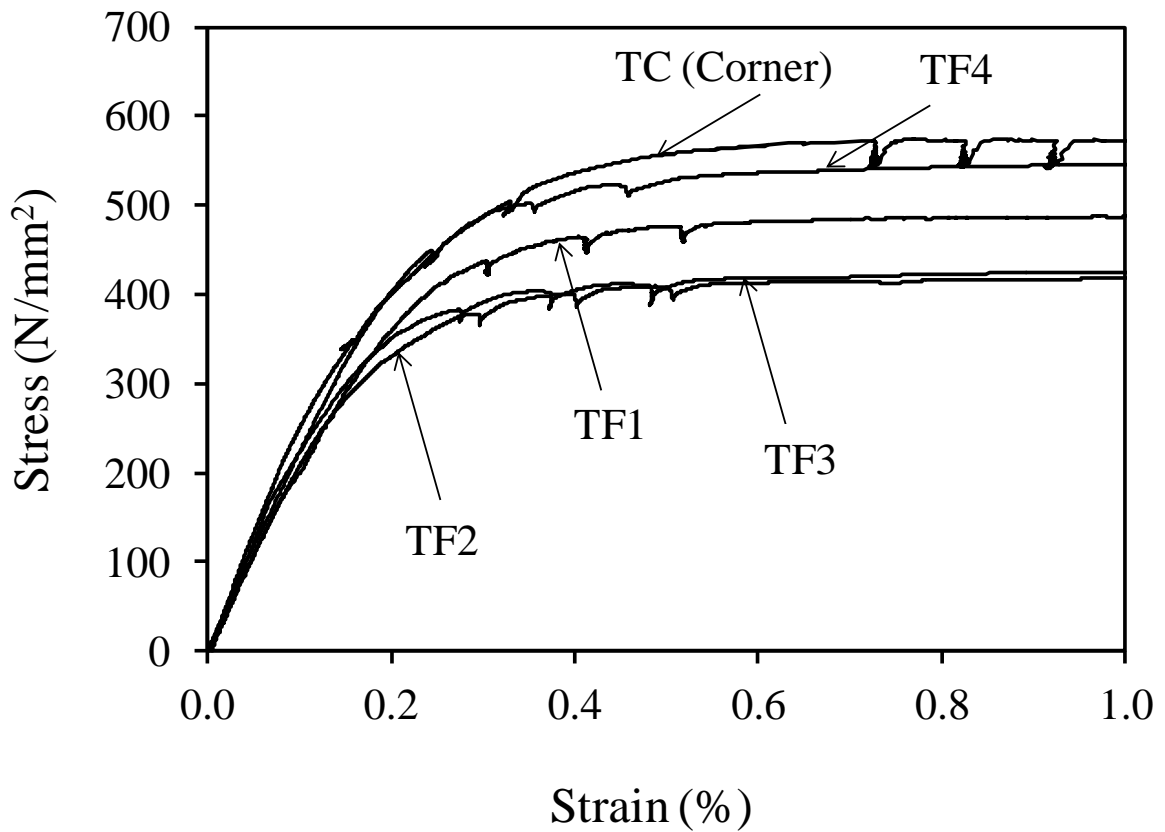


Fig. 2. RHS 120x80x3 tensile stress-strain curves

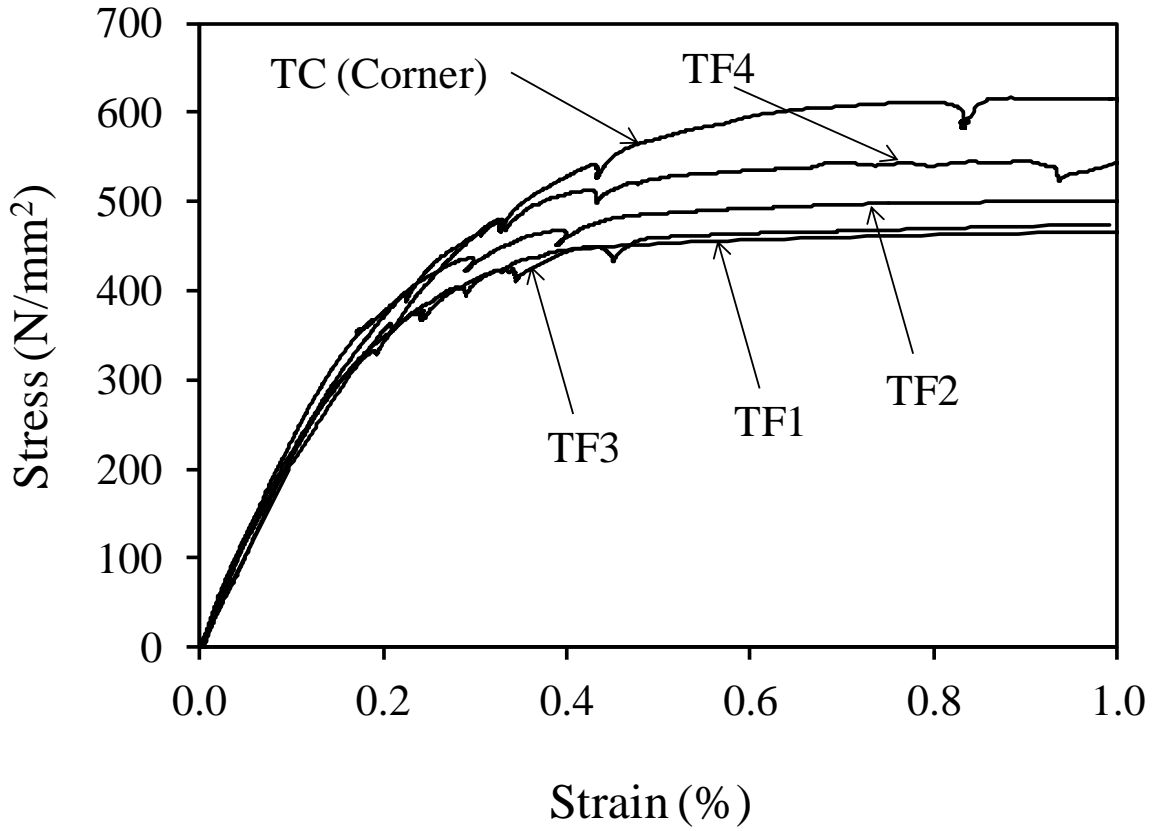


Fig. 3. RHS 60×40×3 tensile stress-strain curves

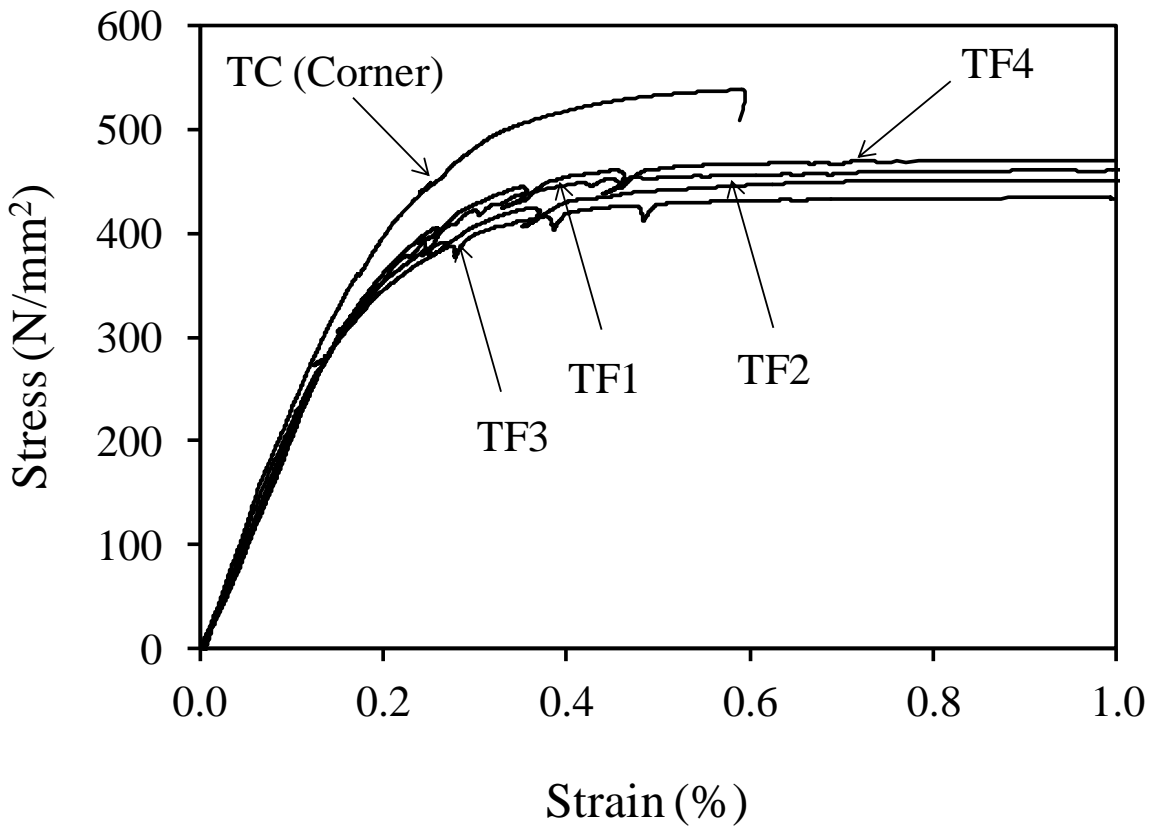


Fig. 4. SHS 80×80×3 tensile stress-strain curves

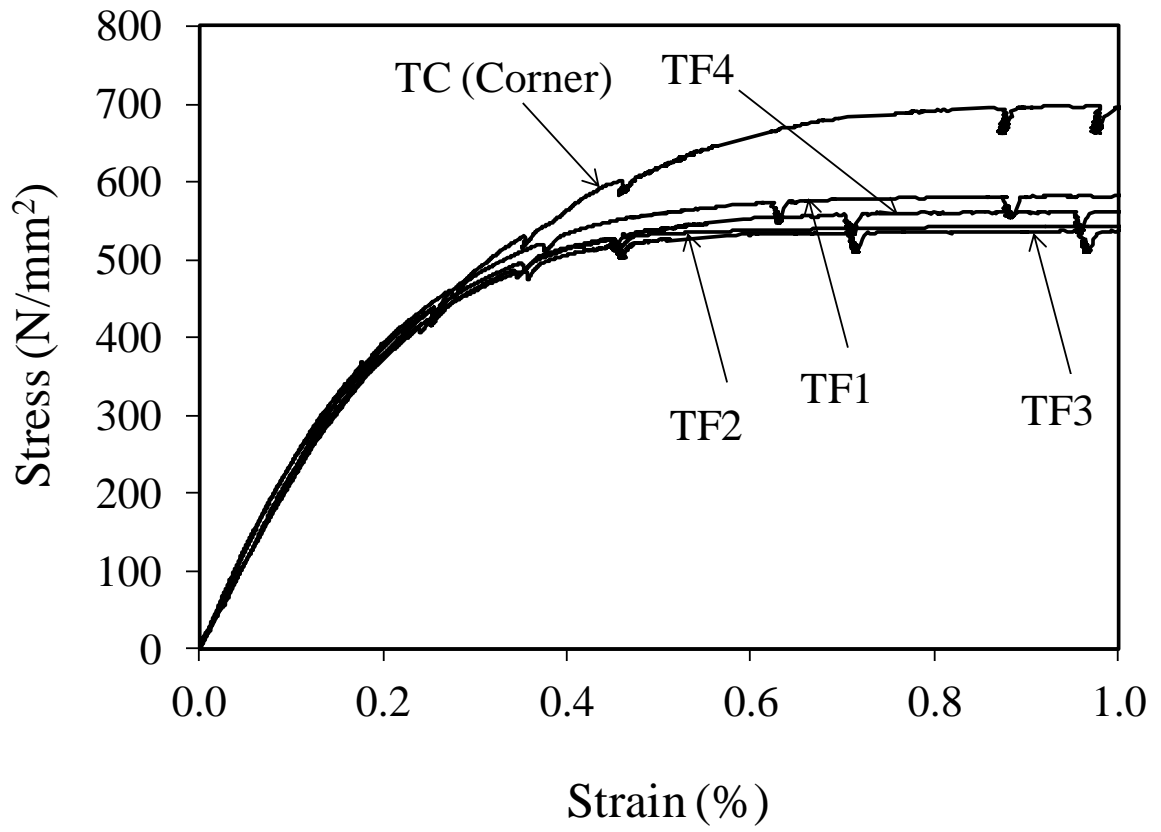


Fig. 5. SHS 60×60×3 tensile stress-strain curves

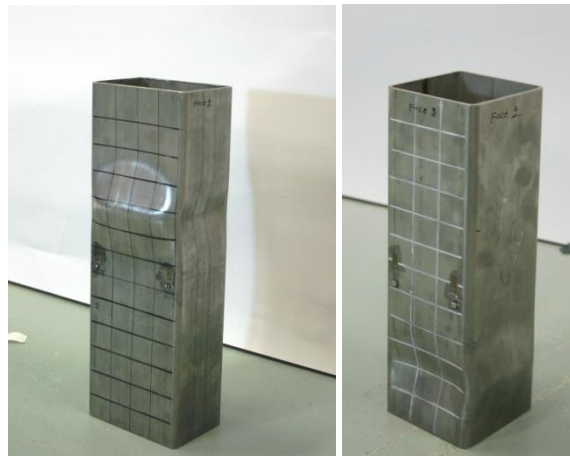


Fig. 6. Typical stub column failure modes

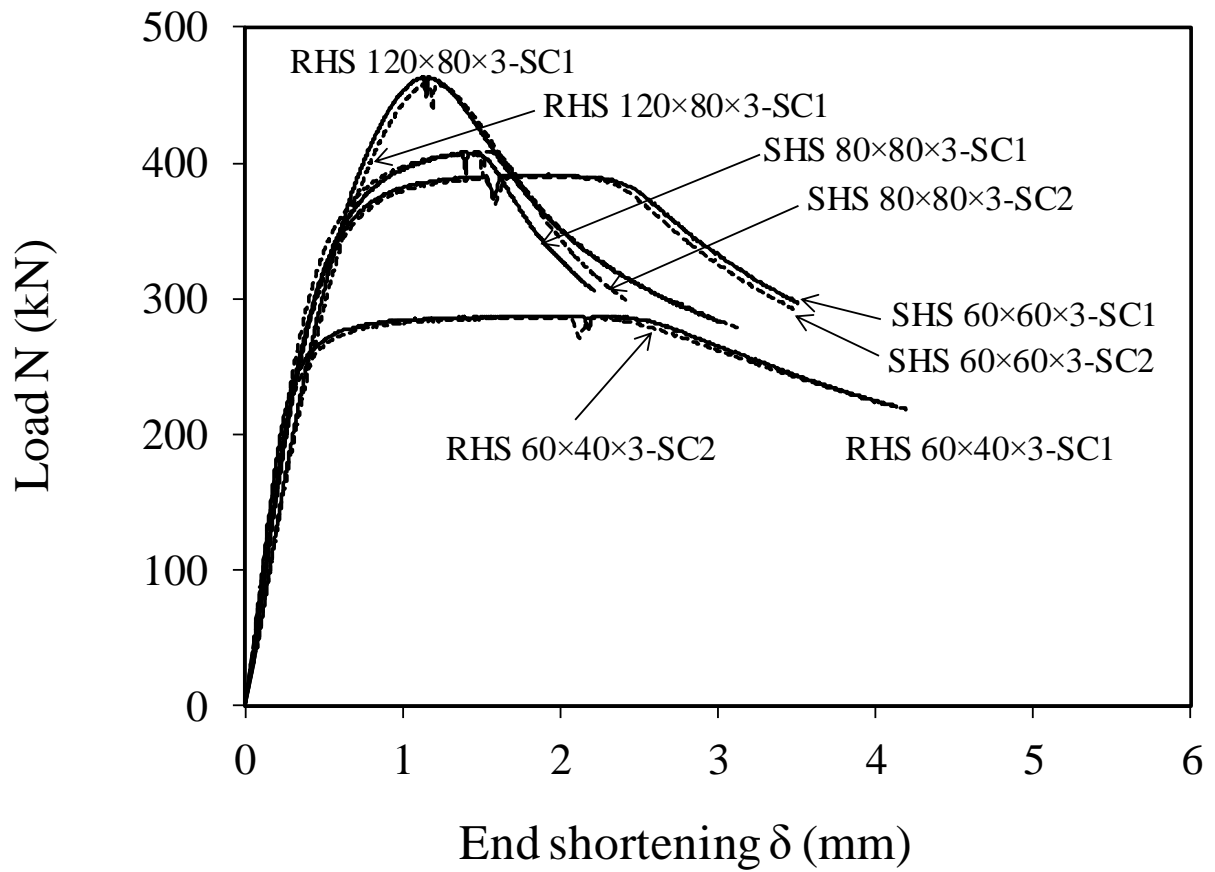


Fig. 7. Load end-shortening curves for stub columns



Fig. 8. Bending test set-up (4PB)



Fig. 9. Bending test set-up (3PB)

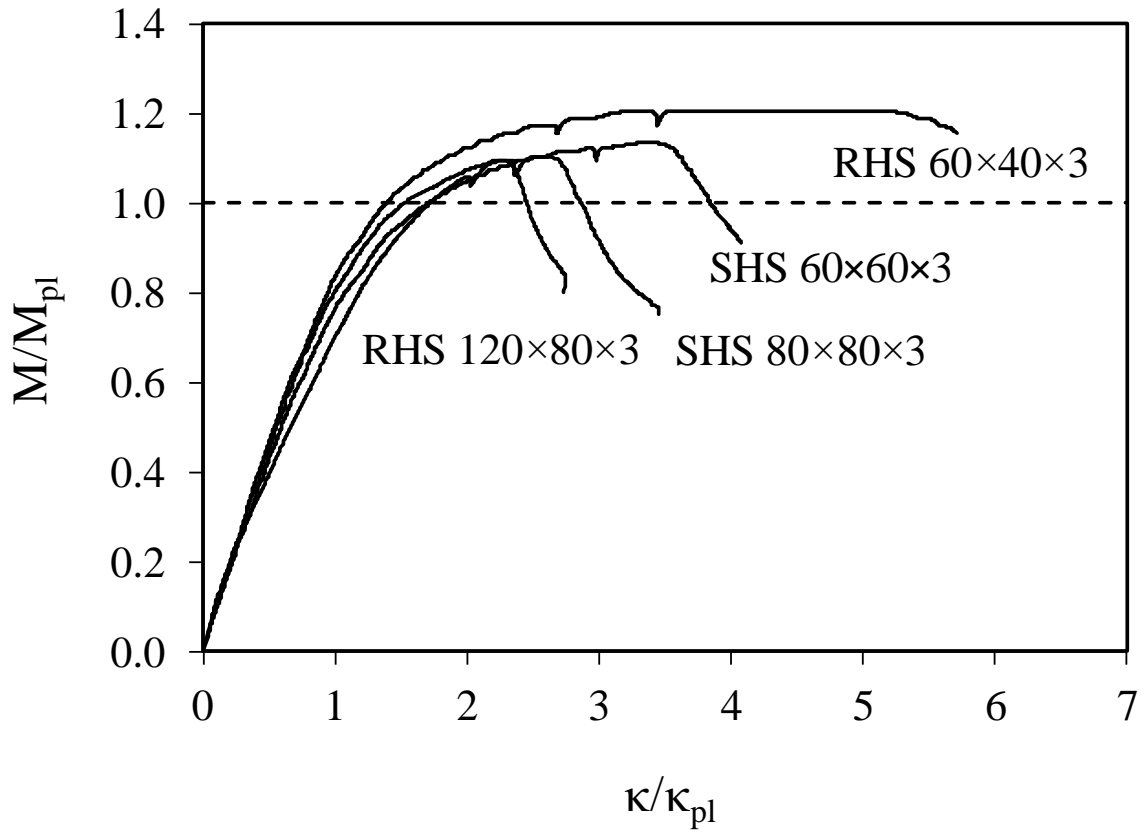


Fig. 10. Normalized moment-curvature results (four-point bending)

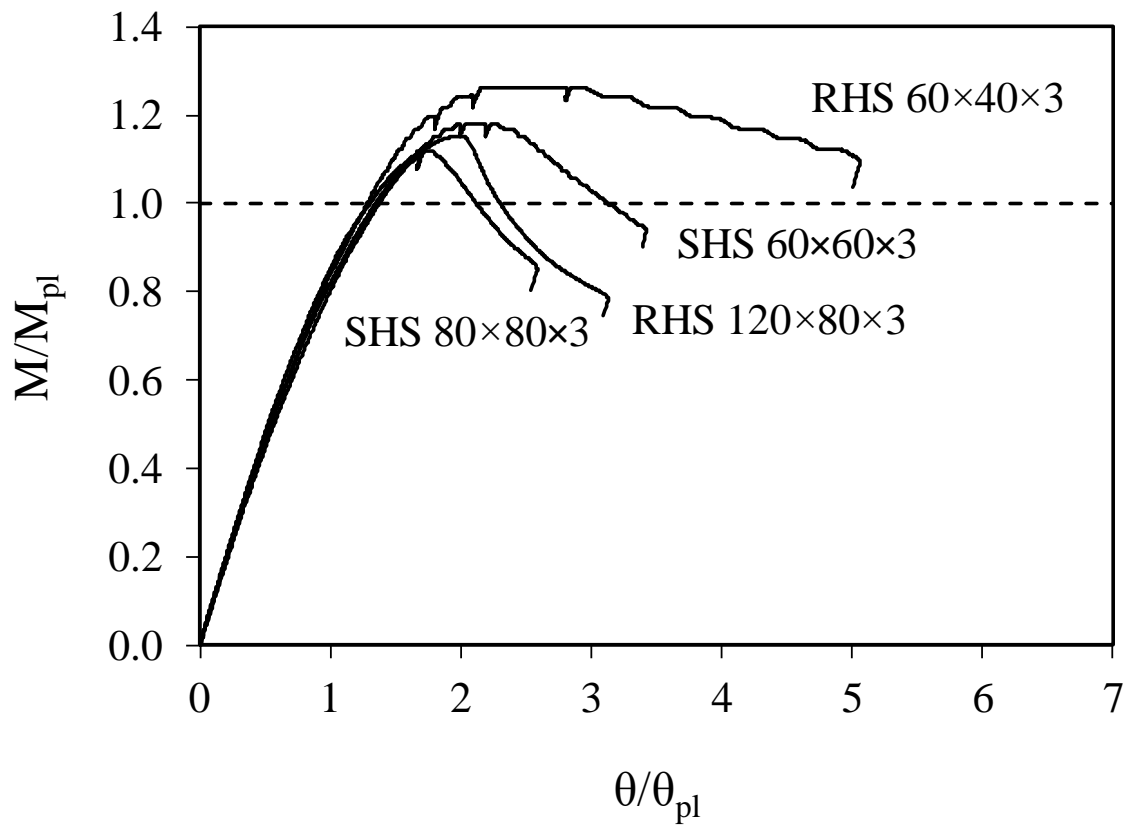
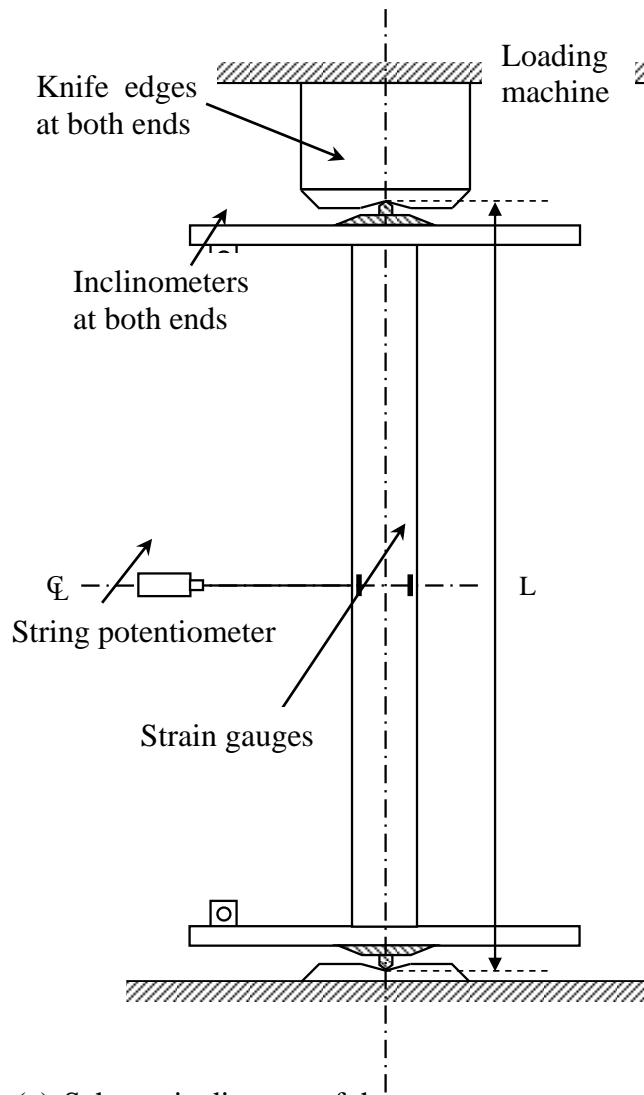


Fig. 11. Normalized moment-rotation results (three-point bending)



(a) Schematic diagram of the test set-up



(b) Experimental set-up



(c) Steel Knife-edge arrangement

Fig. 12. Flexural buckling test set up

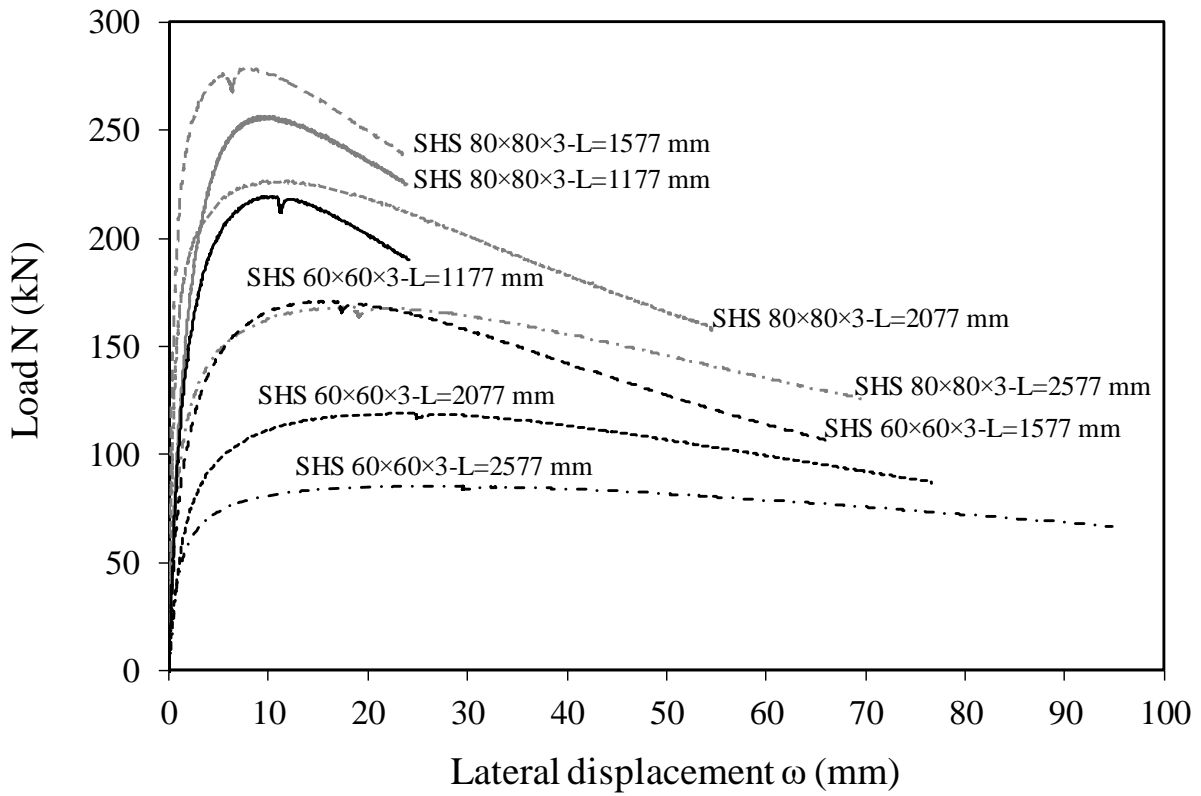


Fig. 13. SHS 80×80×3 and SHS 60×60×3 load-lateral displacement curves

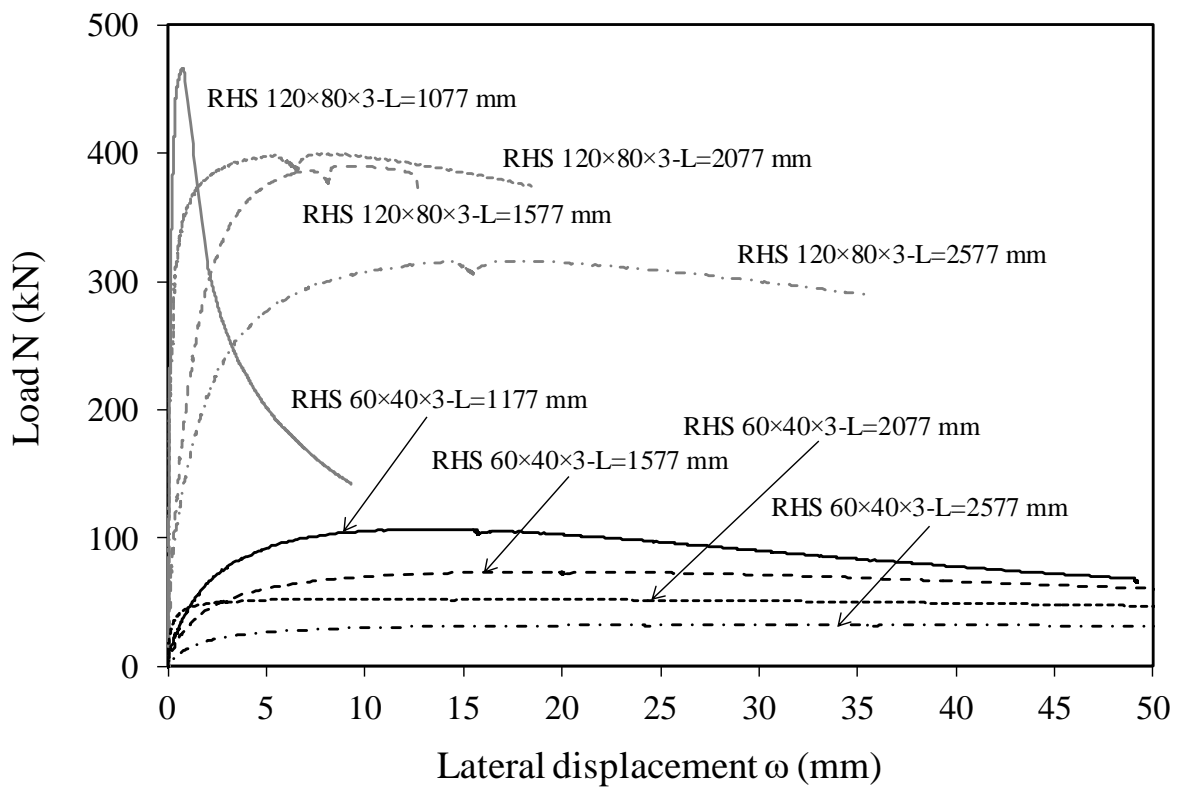


Fig. 14. RHS 120×80×3 and RHS 60×40×3 load-lateral displacement curves

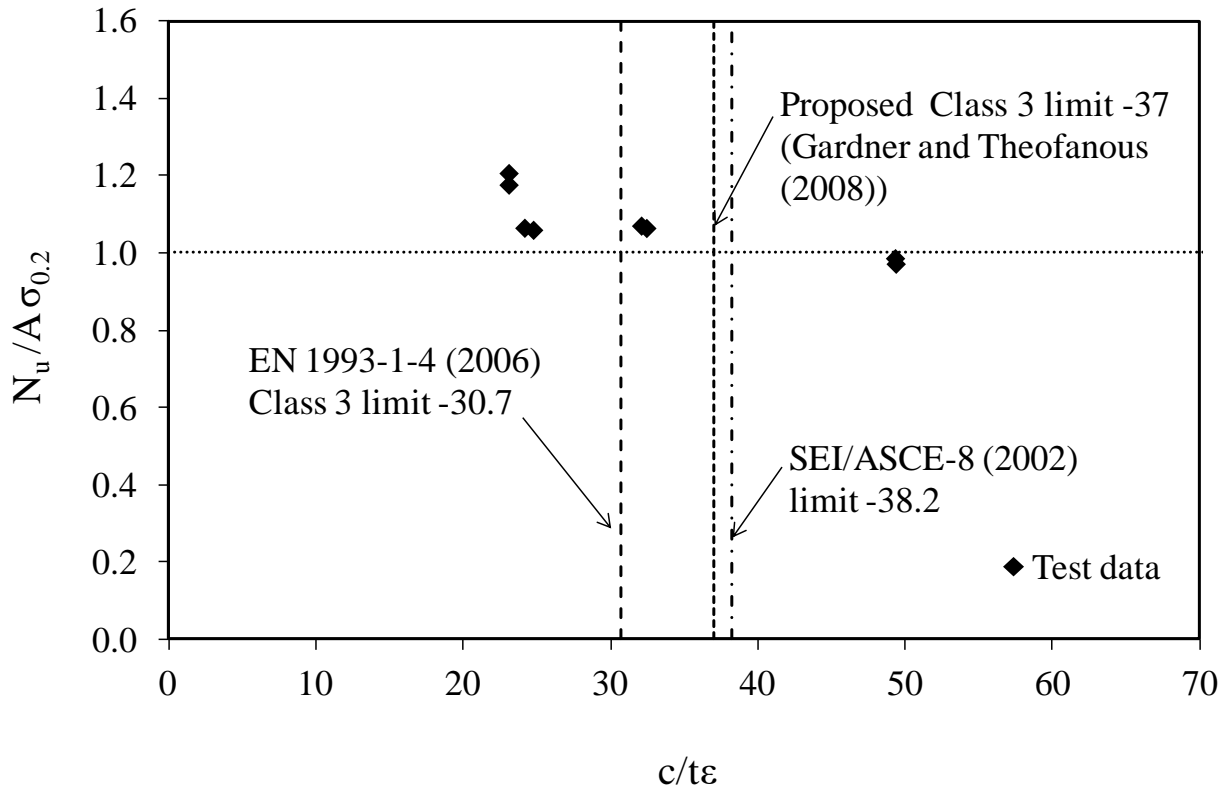


Fig. 15. Assessment of Class 3 slenderness limits for internal elements in compression (stub column tests)

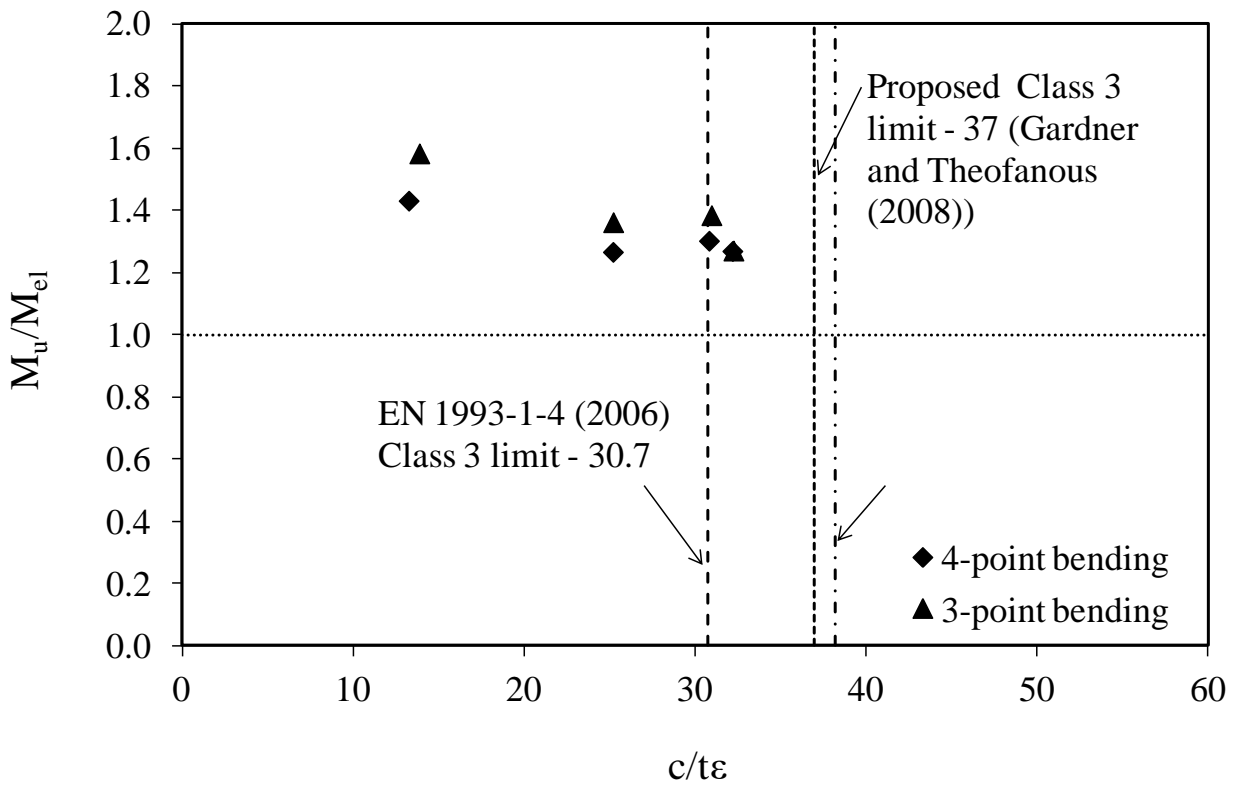


Fig. 16. Assessment of Class 3 slenderness limits for internal elements in compression (bending tests)

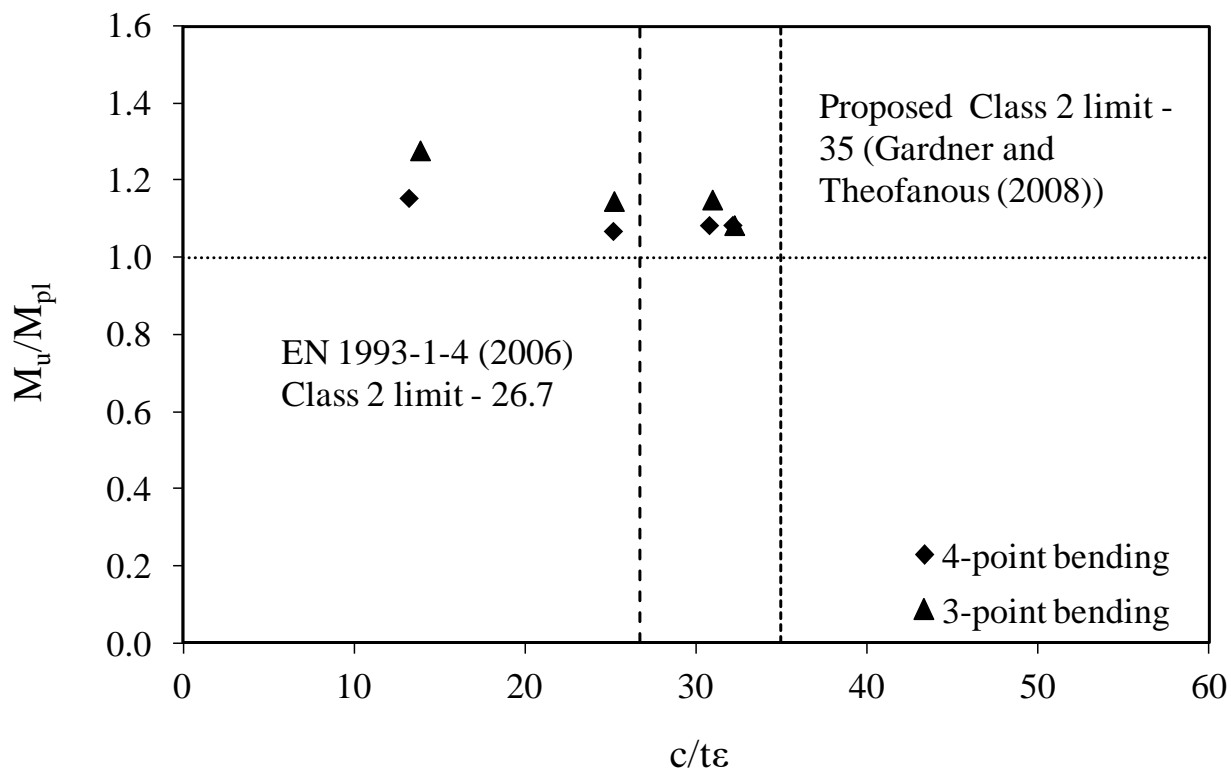


Fig. 17. Assessment of Class 2 slenderness limits for internal compression elements

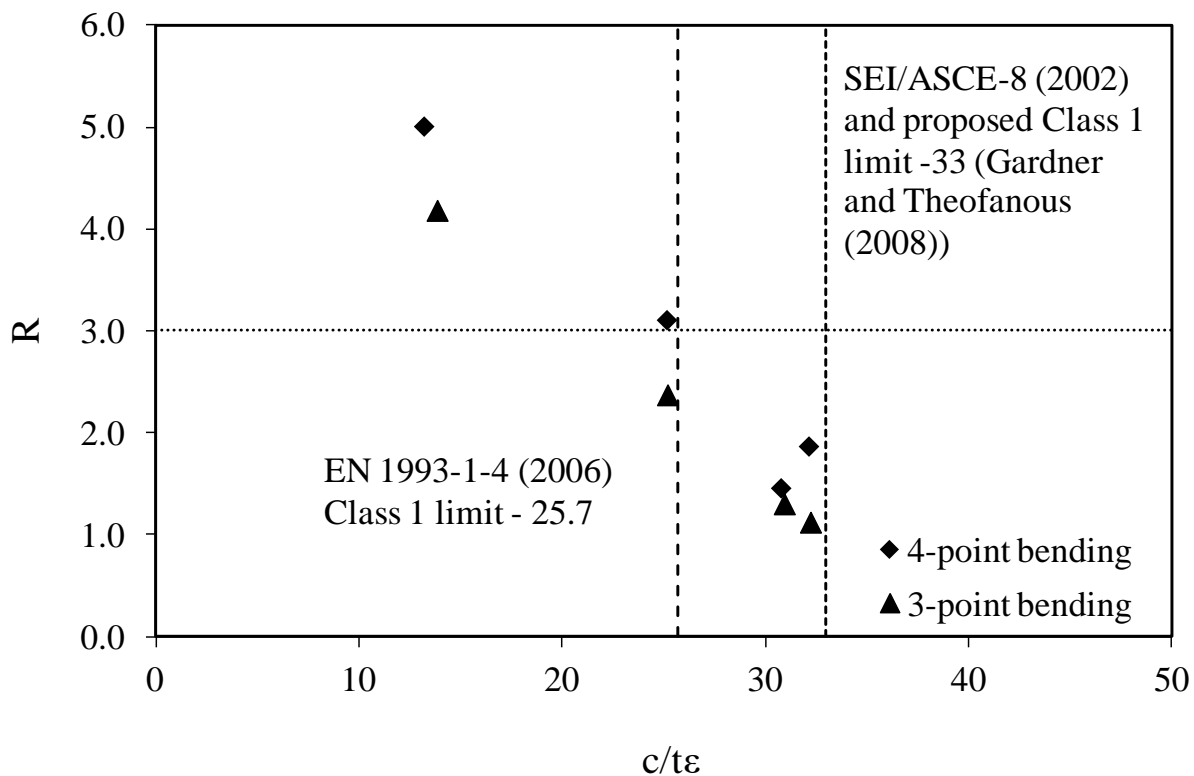


Fig. 18. Assessment of Class 1 slenderness limits for internal compression elements

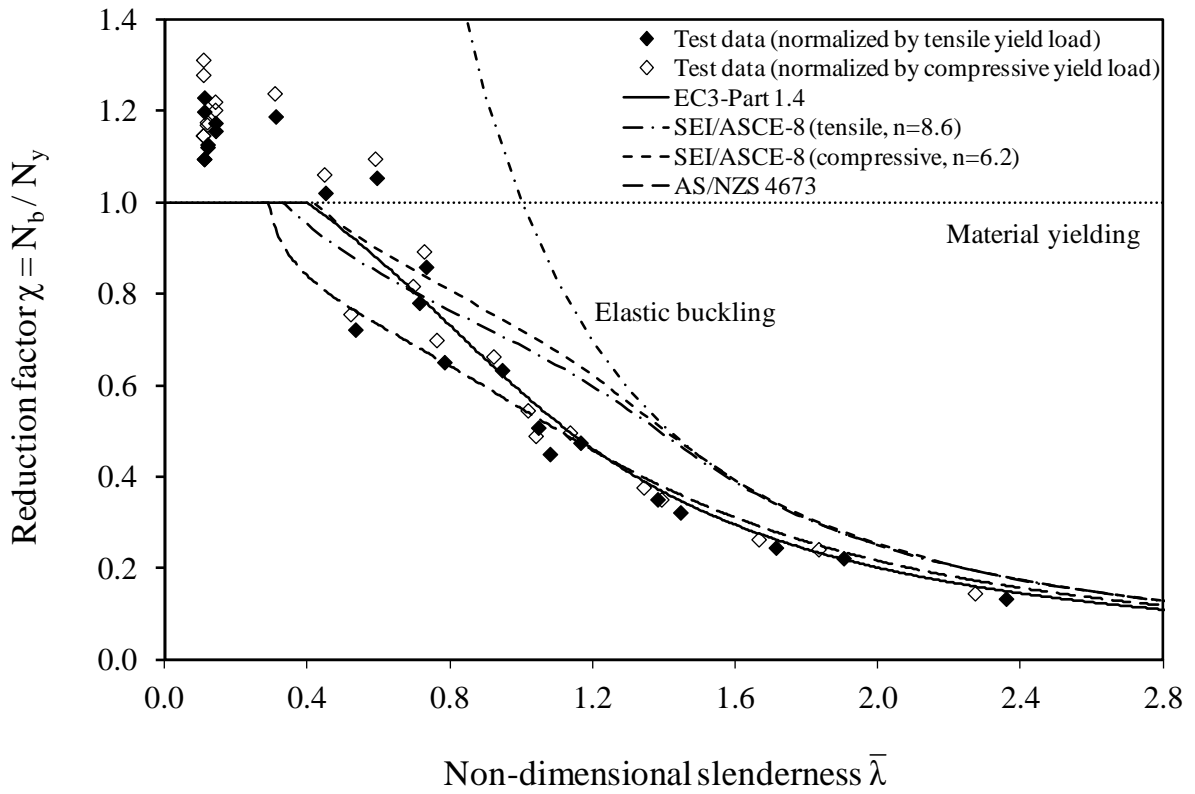


Fig. 19. Flexural buckling test results and code comparisons

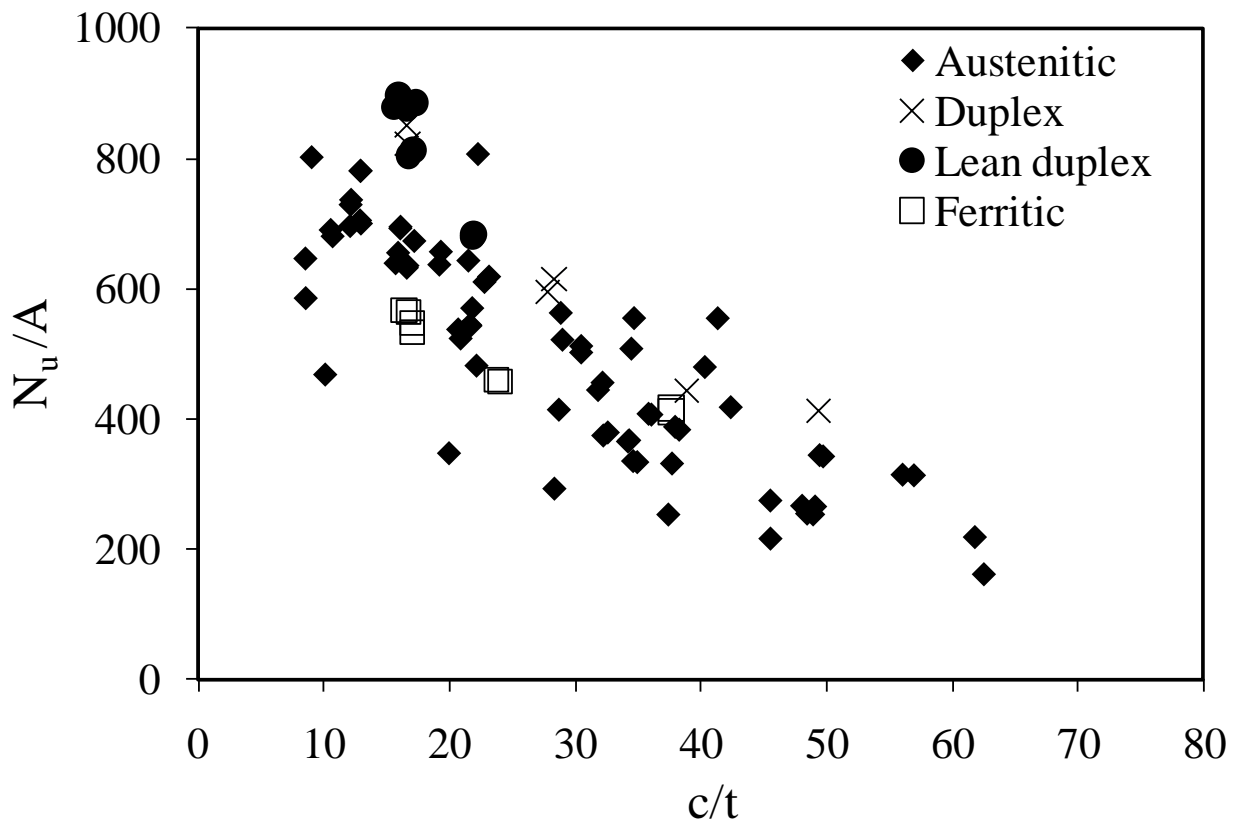


Fig. 20. Performance of stub columns of various stainless steel grades

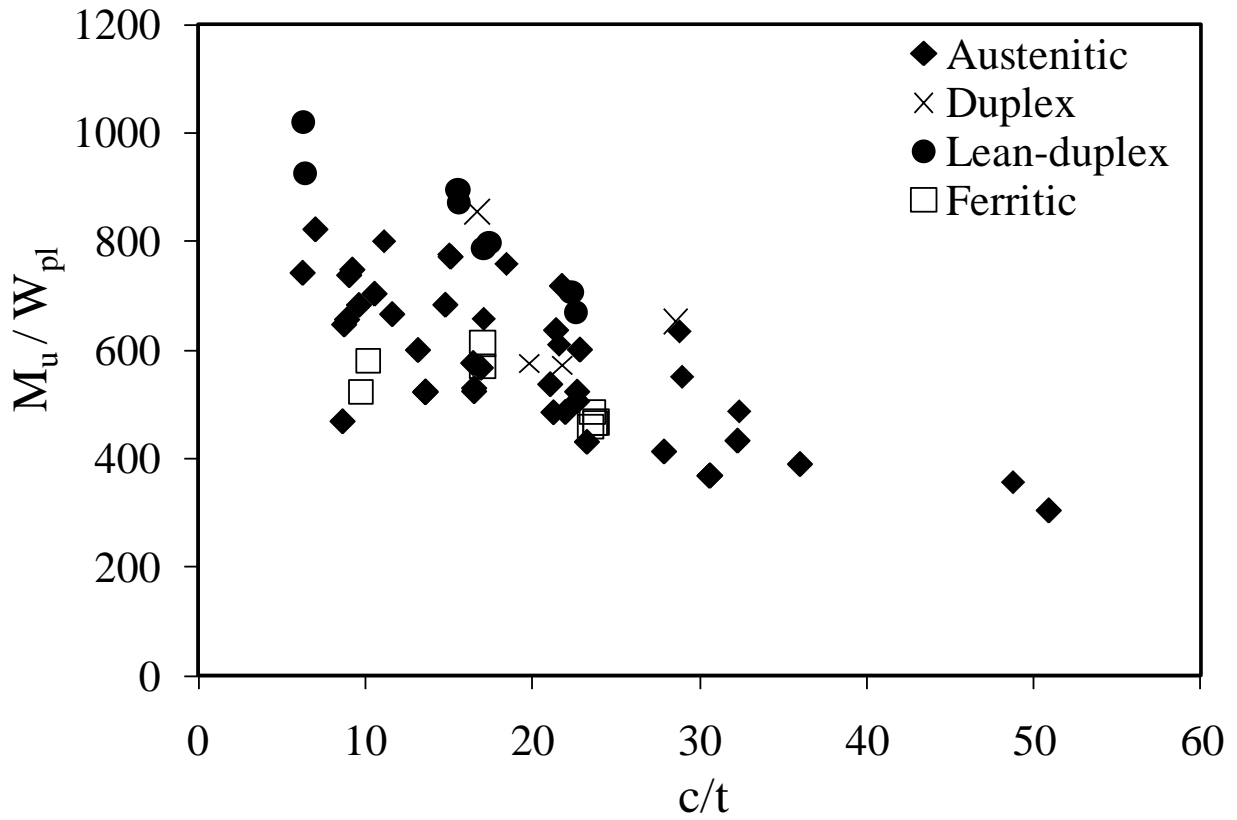


Fig. 21. Performance of beams of various stainless steel grades

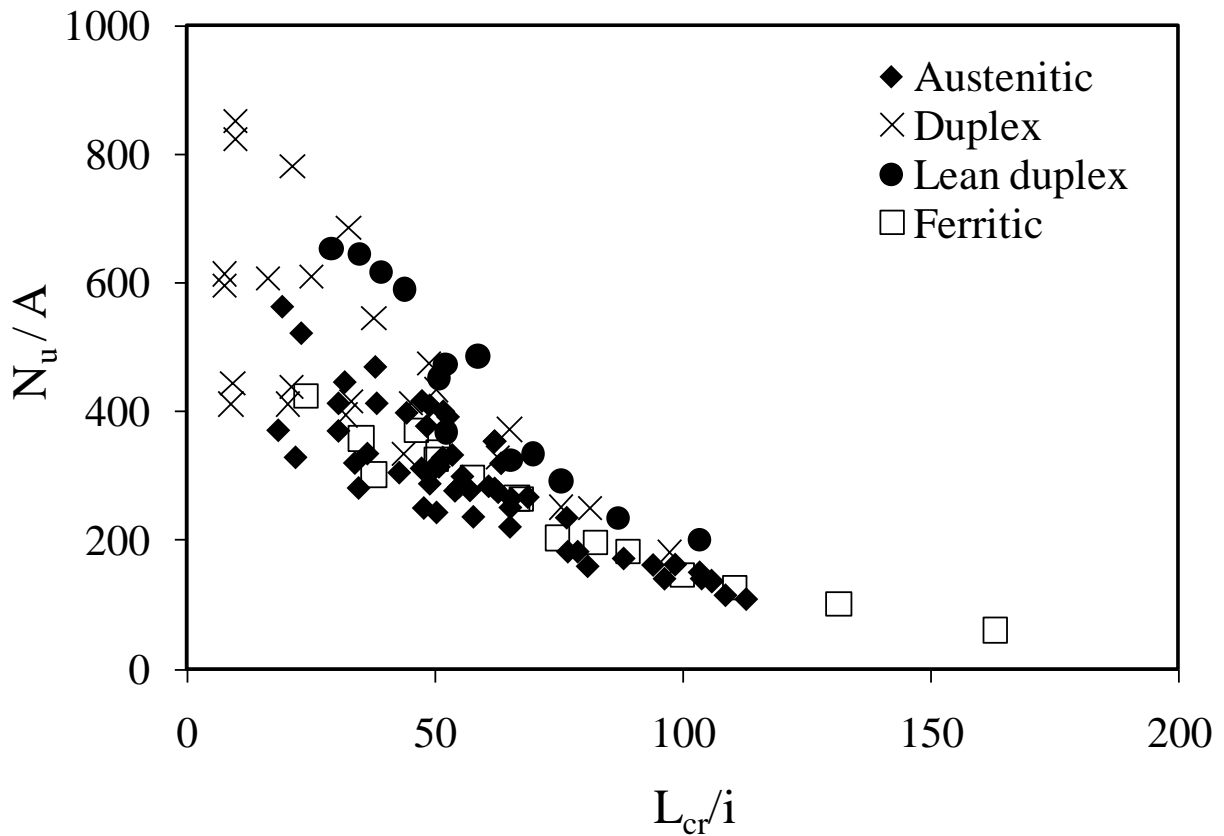


Fig. 22. Performance of columns of various stainless steel grades